A New Method for Spectral Measurements of X-rays From a Laser-produced Plasma Using Differential Absorption

Diploma paper
by
Anna Göransson

Lund Reports on Atomic Physics, LRAP-175
November 1995

ABSTRACT

A new method of spectral measurements of X-rays is evaluated in this work. Different X-ray spectra are reconstructed by looking at the differential absorption in a filter set with elements with nearby K-edges. The filter set is put in front of an image plate which is exposed with X-rays coming from different sources. The image is read out and stored as a digital image. This digital image is converted into numbers and used to make pair-wise subtractions of the transmission values through filters with nearby K-edges. An energy histogram is reconstructed from the subtracted transmission values.

1. Introduction

Research with X-rays emitted from laser produced plasmas has been in progress during a couple of years at the Division of Atomic Physics in Lund. The spectral distribution consists of continuous Bremsstrahlung with a superimposed discrete characteristic line spectrum. It is desirable to know more about the spectral distribution, especially the relation between the continuous spectrum and the characteristic lines. The aim is to optimise the laser system and the process in which X-rays are generated so that the characteristic lines are as intense as possible in relation to the Bremsstrahlung spectrum. The reason is to be able to make sharper images with lower X-ray doses and to achieve X-rays with a higher monochromaticity. One method for measuring the energy distribution from a laser-produced plasma has been to use energy dispersive NaI and Ge detectors. The X-ray emission from a laser produced plasma is pulsed since the laser being used is also pulsed. The laser pulses have a duration of 0.15 ps and the X-rays are emitted during $\approx$1 ps. A lot of photons are emitted during a very short time. The condition on the detector is that only one photon is counted at the time. If several photons are detected at the same time, the detector will simultaneously register the energy of those photons which means that the energy of each photon will be added, leading to *pile-up*. The dead time of the detector is $\approx 1\mu s$ (10^{-6} s) and the X-ray pulse length is $\approx$1 ps (10^{-12} s), hence the detector count at maximum one photon every laser pulse. The optimal counting rate is around one photon every 30th laser shot to make a good spectral measurement. This leads to a lot of usage on the laser equipment and is also impractical since a single radiation target allows production of $\approx$50000 X-ray pulses [1]. The purpose of our new method of spectral measurements which is evaluated in this work, is to be able to measure the energy distribution in a laser produced plasma in one (or few) single shots. A lot of laser time, target material and consequently cost should be saved if this method can be implemented.

2. X-ray emission and absorption

2.1 X-ray emission

X-rays were discovered by W.C. Röntgen in 1895 [2]. They are generated when fast moving electrons bombard a solid. The radiation consists of two parts; continuous Bremsstrahlung and discrete characteristic lines. The Bremsstrahlung is generated when the electrons are gradually decelerated and deflected when passing close to the atomic nuclei in the solid. The energy of the emitted X-ray photon depends on the incoming velocity of the electron and how close to the nuclei it passes (see Fig. 2-1).

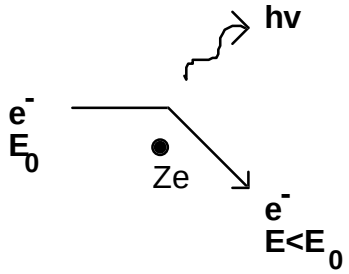

Figure 2-1. An X-ray photon is emitted with energy hv = E_0 - E when an electron with energy E_0 is deflected and slowed down in the field of a nucleus with charge Ze.

When an exciting electron removes another electron from an inner shell, the hole is filled by an outer electron and the binding energy is released as an X-ray quantum. This radiation is discrete and characteristic for every element. Transitions ending in the same shell create a series of transition lines, for example the K, L, M ... series. The transitions can only occur if certain selection rules are fulfilled related to the quantum numbers l (orbital degeneracy) and j (spin-orbit coupling. The rules are $\Delta l = \pm 1$ and $\Delta j = 0, \pm 1$ (see Fig. 2-2).

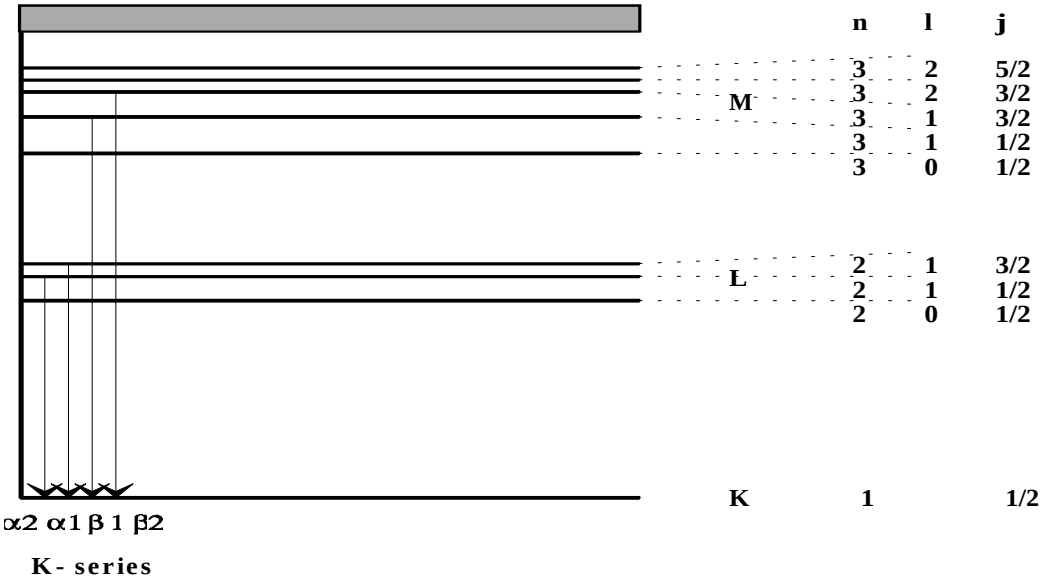

Figure 2-2. Emission lines from the K series in an X-ray spectrum. Each transition emits a characteristic X-ray quantum ($K_{\alpha 1}$, $K_{\beta 1}$, $K_{\alpha 2}$, and $K_{\beta 2}$)

The relation between the wavelength λ of a characteristic line and the nuclear charge Z of the corresponding atom in is given by *Moseley's law,*

$$\frac{1}{\sqrt{\lambda}} = \sqrt{\frac{E}{h \cdot c}} = C(Z - \sigma) \qquad (1)$$

C and σ are constants characterising a particular spectral series, E is the energy of a certain X-ray line, c is the velocity of light in vacuum and h is Planck's constant [3].

Laser produced plasmas

X-rays can be generated in several ways. One of them is to focus an intense laser pulse from a high-power laser onto a small spot of a metal target, creating a plasma. The focal intensity must exceed 10^{11} W/cm^2 if the pulse length is 1 ns. Plasma is matter in a state of ionisation. Characteristics for a plasma are the extreme temperatures (10^6 - 10^7 K), the high ion and electron densities and the highly ionised states. 99 % of all matter in universe is plasma but in our immediate environment plasma is rare. Some plasmas emit X-ray radiation. The plasma-generated X-rays can reach energies in the MeV region depending on the focal intensity and the pulse length of the laser. The spectrum consists of both Bremsstrahlung and characteristic radiation. For each atomic process in the plasma an inverse process exist. For example, the inverse process to Bremsstrahlung is inverse Bremsstrahlung. A photon is then absorbed by an ion-electron system and the electron is raised from a lower level in the continuum to a higher one. The energy of the incoming photon is converted into an increase in kinetic energy of the free electron [3-5]. There are large shot-to-shot fluctuations of the X-ray yield. The reason is fluctuations of the laser plasma, caused by mechanical wobbling of the target, laser intensity and prepulse ratio fluctuations and spatial mode fluctuations due to self-focusing. Examples of modelled laser-produced X-ray spectra from a tantalum and a gadolinium target are shown in Fig. 2-3. The Bremsstrahlung spectrum is believed to be similar for different elements while the characteristic lines depend strongly on the target material [4].

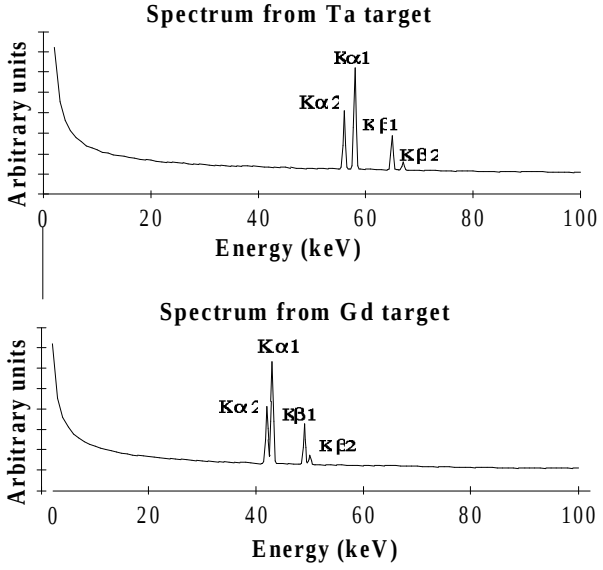

Figure 2-3. Modelled spectra from laser produced plasmas, one with a gadolinium target and one with a tantalum target. The continuous part is the same in the two cases and the emission lines characterise the target material.

2.2 X-ray absorption

The X-ray absorption depends on both the energy of the incoming X-rays and the atomic number of the absorber. The attenuation in an element decreases monotonous with photon energy until the photon energy is high enough to remove an electron from one of the shells. At this energy level, called absorption edge, the absorption increases abruptly because ionisation from a new inner shell is permitted. The energy of the absorption edge is equal to the binding

energy of the released electron. The absorption edges are denoted with the symbols K, L_I, L_{II}, L_{III}, M_I, M_{II} etc. depending on from which electron shell an electron is removed (see Fig. 2-4). The absorption coefficient, μ, is a function of X-ray energy (E) and atomic number (Z),

$$\mu(Z,E) \cong \frac{Z^{\alpha}}{E^{3}} \qquad 3 \le \alpha \le 4 \tag{2}$$

between the edges [6]. The unit of the absorption coefficient is often cm^{-1}. The absorption coefficients for two different elements as a function of photon energy are shown in Fig. 2-6.

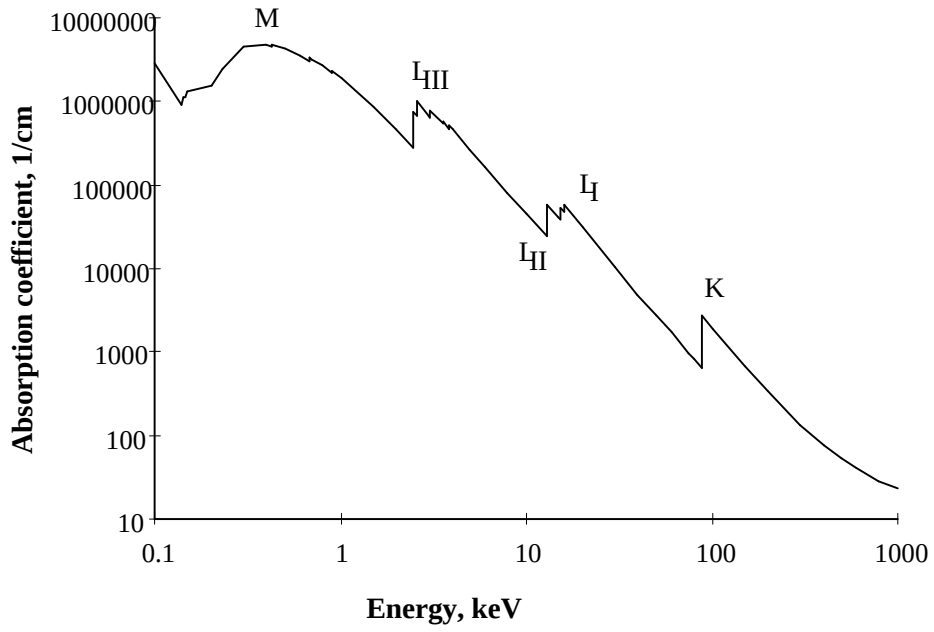

Figure 2-4. X-ray absorption spectrum from lead with absorption edges $K, L_{III}, L_{II}, L_I, M_I$. The absorption coefficient falls off as a function of E^{-3} between the edges.

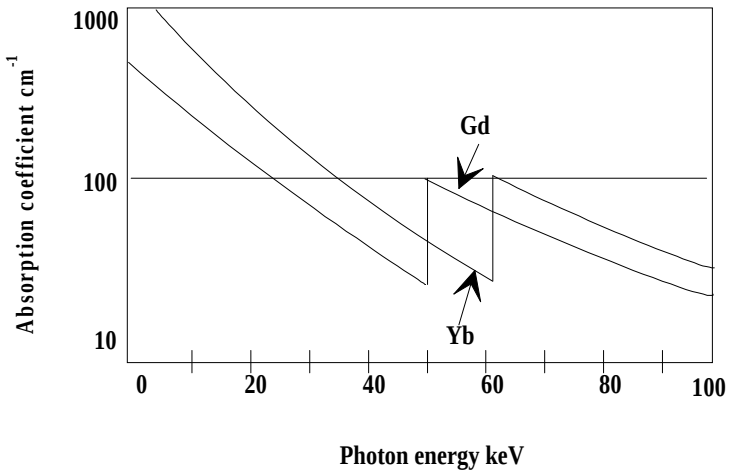

Figure 2-5. The absorption coefficient as a function of photon energy in the energy interval 20 - 100 keV. The elements are Gd and Yb. Note that the attenuation coefficient of gadolinium is greater than that of ytterbium in a small energy region even though the atomic number of ytterbium is higher.

The attenuation in an element occurs via Compton scattering and photo conversion in the energy region 20 - 100 keV, which is the energy range of interest in this work. The attenuation is described by the Beer-Lambert law: $I(Z,E) = I_0 \cdot e^{-\mu(Z,E)\cdot x}$ (3) where I is the intensity after attenuation, I_0 the incoming intensity and x the thickness of the absorber.

3. Differential absorption

3.1 Method

The method of spectral measurements, evaluated in this work, employs the fact that an element has a unique absorption coefficient which is a function of energy. A spectrum is reconstructed by subtracting the value of the X-ray transmission through two foils, made from elements with nearby K-absorption edges and adapted thickness. Adapted thickness means that the transmissions of the two foils are the same before and after the K-edges, respectively (see Fig. 3-1).

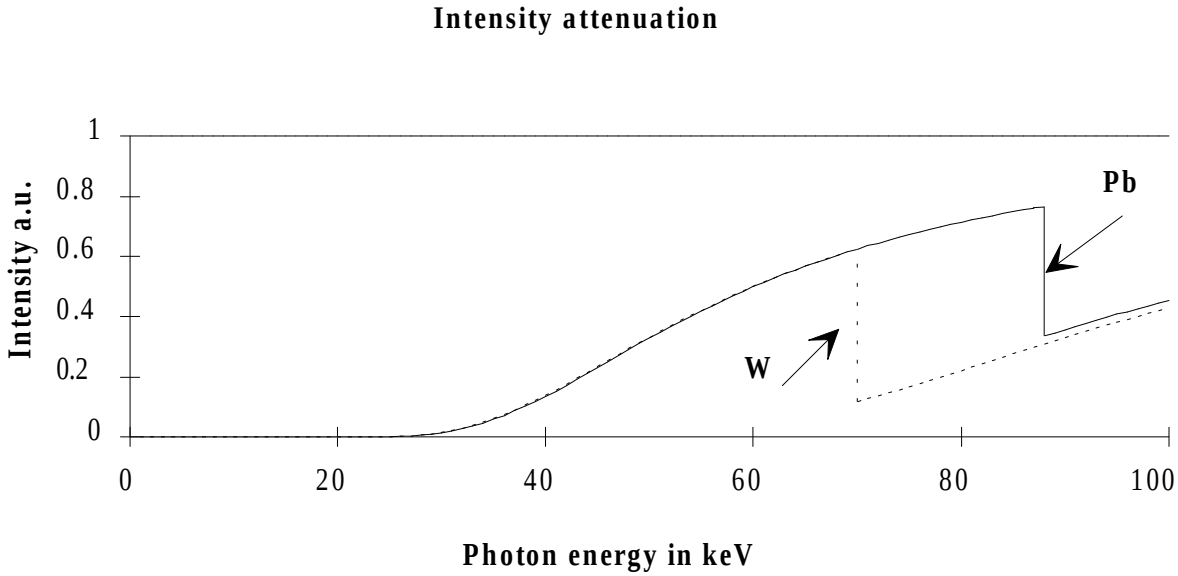

Figure 3-1. Transmission curves of two elements, W and Pb, with adapted thickness. The curves overlap before the first K-edge and after the second K-edge which means that the transmission is almost the same here.

The difference gives information about the total attenuated intensity in the energy interval given by the K-edges, since the difference is almost zero outside the interval because of the adapted thickness. The spectrum is examined in an increasing energy range by repeating this action for elements with increasing atomic number (i.e. increasing K-edges) (see Fig. 3-2). The attenuation in an interval is given by the attenuation coefficient of the two elements and the resolution is given by the number of elements used and the separation between their K-edges. If the energy separation is 5 keV then the resolution is 5 keV. Each subtraction examines a small interval of the spectrum determined by the energy interval of K-edges (see Fig. 3-3).

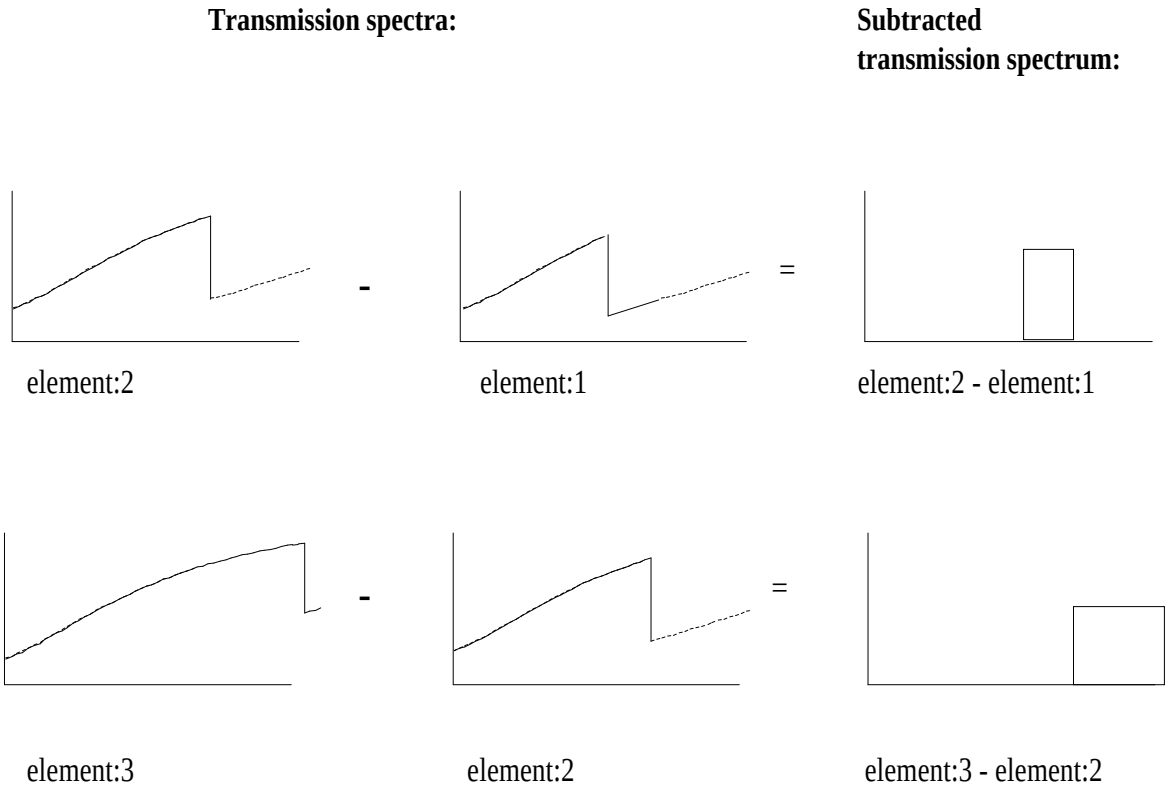

Figure 3-2. The figure shows pair-wise subtraction of the transmission spectra through three elements with adapted thickness. The horizontal axis denotes energy and the vertical axis denotes the relative intensity.

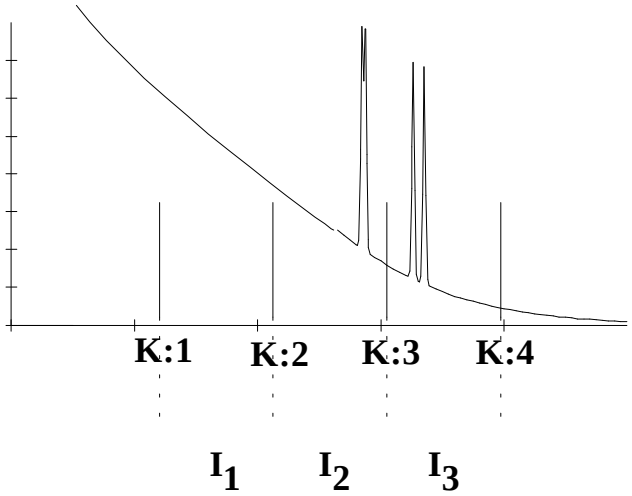

Figure 3-3. A spectrum is divided in 3 interval (I_1 -I_3) determined by the energy position of the K-edges of four elements (K:1-K:4).

3.1.1 Spectrometer

The spectrometer, which we want to develop, consists of a set of elements with nearby K-edges and matched thickness and an image plate (IP) described in Sect. 4. An X-ray yield, passing through the set of elements, exposes the IP. The blackness of the IP, meaning the

accumulated X-ray dose in the IP, gives information about the total transmission through an element, i.e. the integral of the transmitted spectrum. Subtracting two blackness values gives the integrated intensity in an energy interval defined by the position of the K-edges. This integrated intensity is used for reconstruction of an energy histogram with bin widths determined by the K-edges of the elements used (Fig. 3-4).

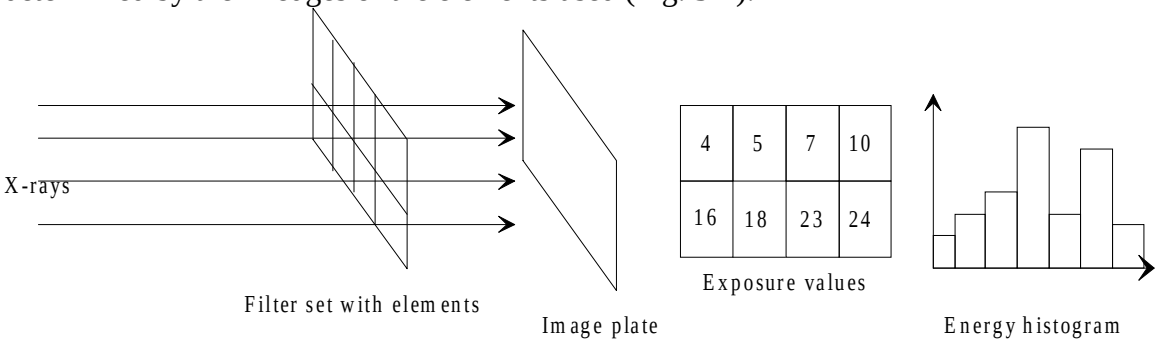

Figure 3-4. Illustration of the spectrometer which is going to be developed.

3.1.2 Source Spectra

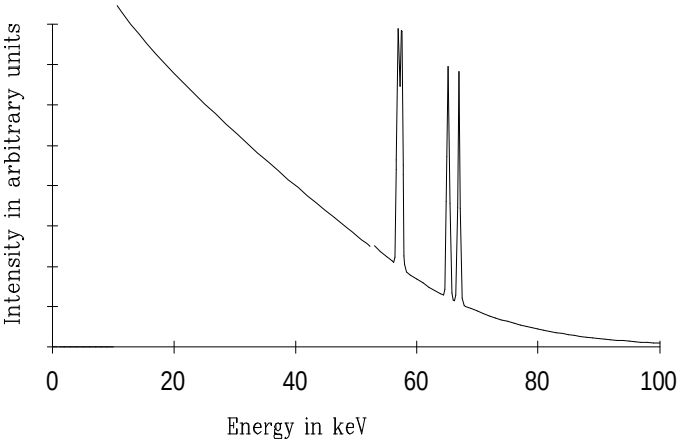

Figure 3-5. A modelled spectrum from a tantalum plasma.

A laser produced plasma from a tantalum target is the X-ray source (see Fig. 3-5). The spectrum consists of a continuous Bremsstrahlung spectrum and some characteristic lines ($K_{\alpha 2}$, $K_{\alpha 1}$, $K_{\beta 1}$, $K_{\beta 2}$) with the energies 56.3, 57.5, 65,2 and 67.0 keV. There are problems with fluctuations of the laser plasma which lead to fluctuations of the intensity in the emission lines (see Sect. 2.2).

3.1.3 Transmission spectra

Elements with K-edges in the energy range of the emission lines of tantalum are examined. It is desirable to find elements with K-edges between and outside the interval defined by those lines. Possible elements (in theory) and their K-edges are shown in Table 3-1.

Atomic number	64	65	66	67	68	69	70	71	72	73	74	75
Element	Gd	Tb	Dy	Ho	Er	Tm	Yb	Lu	Hf	Ta	W	Re
K-edge (keV)	50.2	52.0	53.8	55.6	57.5	59.4	61.3	63.3	65.3	67.4	69.5	71.6

Table 3-1. Possible element to use for differential absorption to examine the characteristic lines in tantalum.

Choosing four elements with K-edges below, above and between the K_α and the K_β lines and adapting their thickness so they have the same transmission before their K-edges it should be possible to have a rough estimation of the energy content in the K_α and K_β line. This hypothesis is tried in theory. The chosen elements are lead, ytterbium, gadolinium and cerium. Their thickness are adapted in one point before the K-edges of all three elements. The transmissions of a tantalum spectra through the elements are shown in Fig. 3-6. The subtracted transmission spectra are shown in Fig. 3-7. In practice those spectra are histograms looking like the one shown in Fig. 3-8.

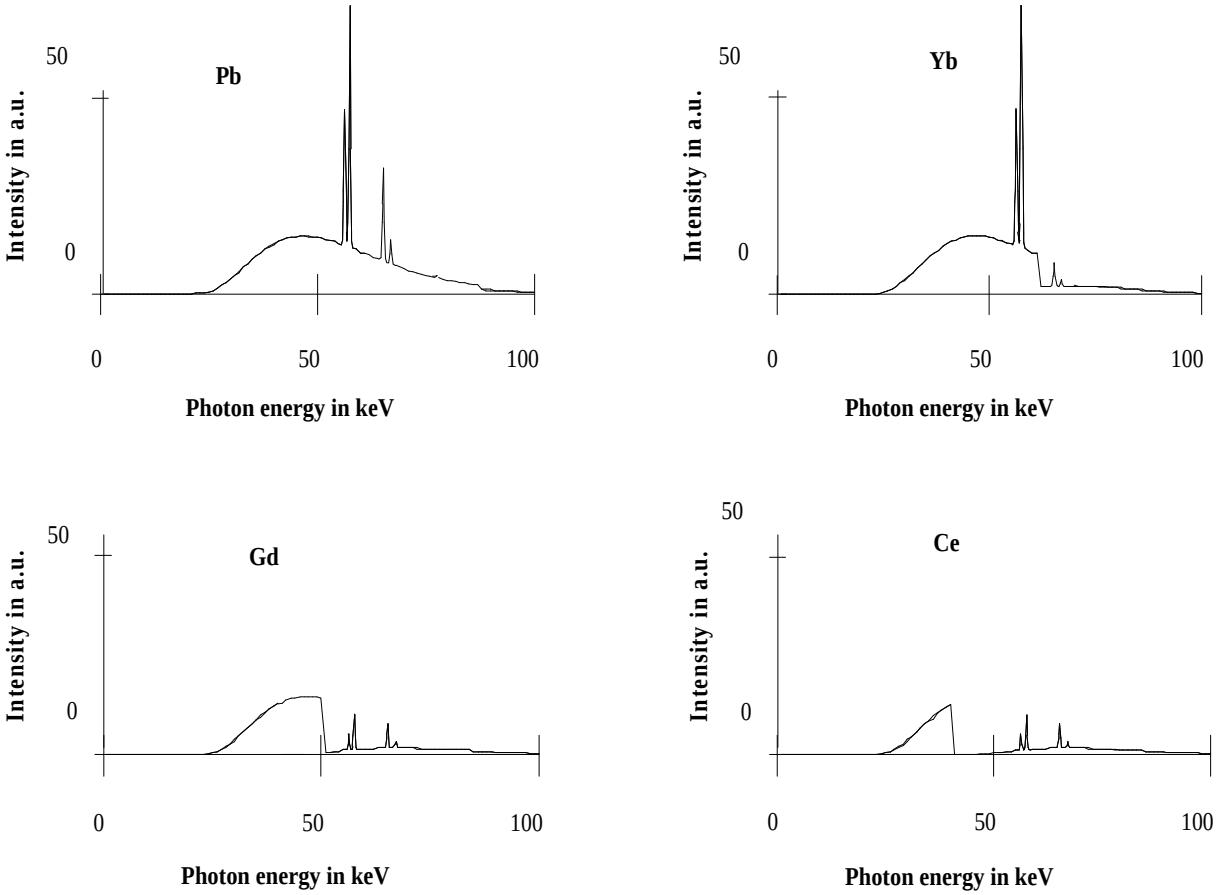

Figure 3-6. The diagrams show the transmission spectra through lead, ytterbium, gadolinium and cerium filters. The thickness are adapted pair wise, i.e. lead and ytterbium, ytterbium and gadolinium and gadolinium and cerium are adapted to each other.

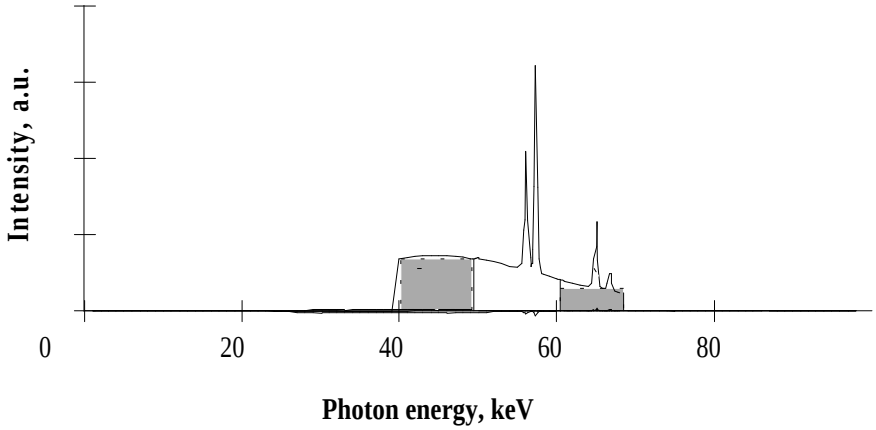

Figure 3-7. The first area (///) shows the subtraction of a Gd and Ce transmission spectra. The second area (transparent) shows the subtraction of a Yb and Gd spectra. The third area (\\\) shows the subtraction of a W and Yb transmission spectra.

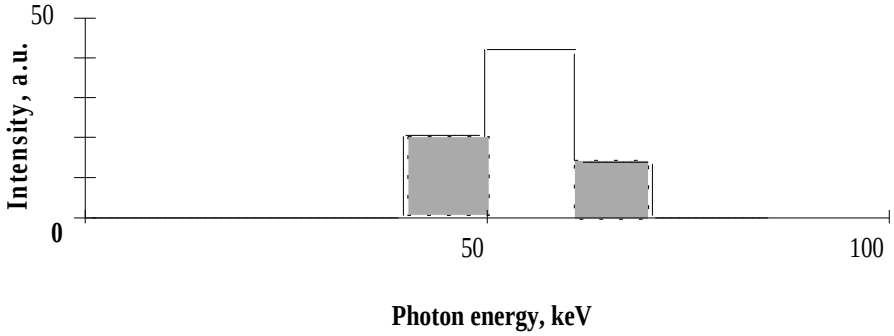

Figure 3-8. The areas with the same pattern in Fig. 3-7 and 3-8 correspond to each other.

4. Image plate

4.1 Theory

4.1.1 Image plate

The Image Plate, (IP), is composed of three layers; a protective layer (10 μm), a photo-stimulable crystal layer (150 μm) on a polyester support layer (250 μm) (Fig 4.1).

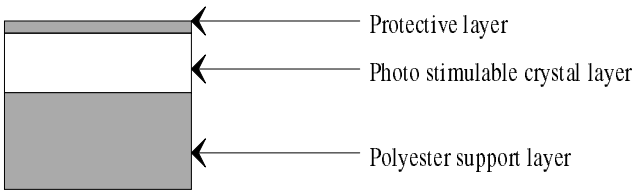

Figure 4-1 Composite structure of the imaging plate

The crystal layer consists of europium-doped barium fluorohalide compounds, BaBrFI: Eu^{2+}, where the europium works as a luminescence centre. The X-ray energy is stored in colour centres when the IP is exposed. When the IP is scanned with a He-Ne-laser (633 nm) the photo-stimulable layer is excited and release the stored energy by emitting luminescence light (PSL = Photo Stimulated Luminescence). The wavelength of this PSL-light is 400 nm. The PSL light is collected with a light guide and converted to electric signals in a photo multiplier tube. These signals are digitised and a digital image is created. The IP is reusable. The residual energy will be erased by flooding the IP with visible light. There are a lot of advantages with IP compared to other radiation image sensors, such as high sensitivity, wide dynamic range (10^4-10^5), superior linearity; the fluorescence emission is proportional to the dose in the entire range and the accumulated background radiation can be erased before use [7].

4.1.2 Digitising unit

We use the Bio-Image Analyser BAS2000 (Fuji Film Co.,Ltd) to analyse the IP. This system consists of an image reader, an imaging processor, an IP eraser and a printer. The image reader reads the stored information with help of a He-Ne laser which stimulates the crystals to emit photo stimulated luminescence (PSL). The PSL light is collected by a light collection guide and amplified in a photomultiplier tube. The light is converted into electric signals which are digitised. The imaging processor, provided with a 32-bit work station, records, displays and analyses radiation image data. The IP eraser erases the stored information by flooding the IP with visible light [7-8].

4.1.3 Image analysis

The digital image from the BAS 2000 is stored in 10 bit-format. The format is called img-format. The blackness, measured in QL values (= Quantisation Level) varies from 0 to (2^{10}-1). The quantisation level is the digitised value corresponding to the number of photons that reach the IP. The QL value is proportional to the logarithm of the PSL value and the PSL value is proportional to the number of photons reaching the IP i.e. to the incoming intensity. The image is truncated with a computer programme into 8 bit format (bmp-format) which is more useful with the software that is available. The blackness is here measured in pixel values which vary from 0 to 2^8-1. Since we are interested in the PSL values which are proportional to the exposure of the IP and also the incoming X-ray intensity, we must use the following relations:

$$PSL = const \cdot 10^{l\cdot(\frac{QL}{N} - \frac{1}{2})} \quad (4)$$

$$QL_{bmp} = 255 \cdot \frac{(QL - QL_{\min})}{QL_{\max} - QL_{\min}} \quad (5)$$

QL_{bmp} = the pixel value (0-255) representing the blackness from the 8 bit picture,
Ql_{max} and $QL_{\min}$ are the upper and lower value (between 0 and 1023) that are used for truncation of the image data from 10 to 8 bits with a conversion programme.
The overall dynamic range of the image plates is larger than what can be handled by the image reader. The reading interval of the scanner is controlled by setting two parameters (*s* and *l*) to certain values. How to choose those values depends on the exposure and the sensitivity range (Fig. 4-2).

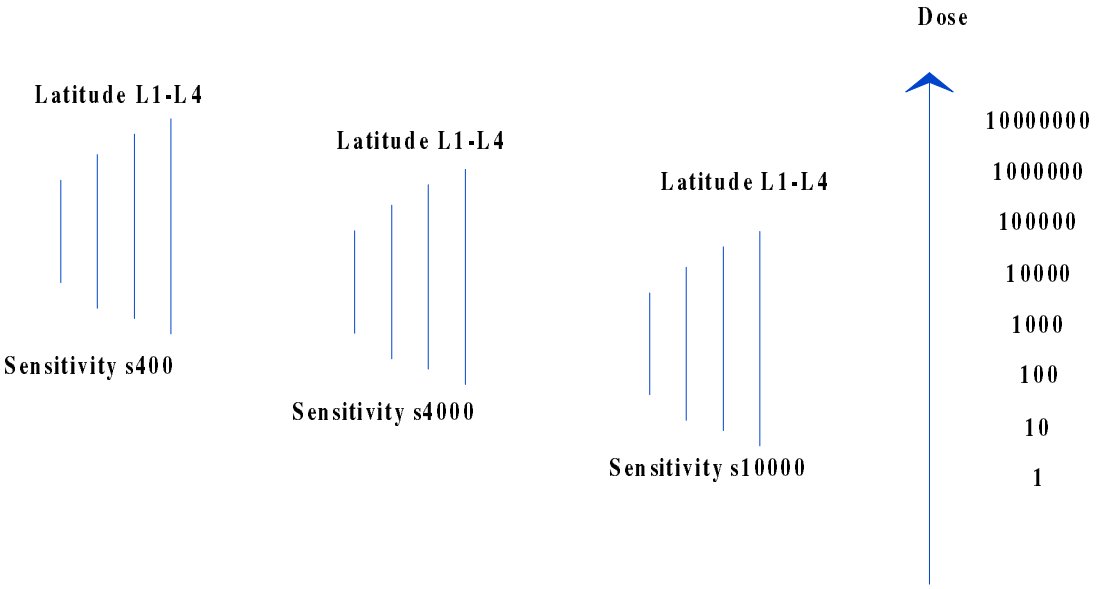

Figure 4-2. The sensitivity of the IP varies with the exposure dose. It is possible to chose different combinations of sensitivity and latitude. The larger latitude that is chosen the wider the dose range gets i.e. the IP is sensitive in a wider dose range.

s = sensitivity, *l*= latitude (values you choose when you scan the IP at the BAS 2000), *const* = 10000/ *s*, *N* = 1024 (number of grey scale levels)

4.2 Analysis of the image plate with respect to sensitivity and accumulated background

Some exposures of the IP were made, first with only background radiation and second with a mono energetic source of iodine with varying exposure times. The reason was to verify that the PSL value is a linear function of the dose (exposure) and to see how much the background radiation affect the total blackness of the IP. Hence, it is possible to subtract this offset value from the total blackness. It is also necessary to be able to estimate the variation of the pixel values, i.e. the standard deviation

4.2.1 Experiment

4.2.1.1 Iodine

In test experiments we used a radioactive iodine source. ^{125}I decays by electron capture into excited ^{125}Te. 35 keV X-ray photons (7%) and conversion electrons (93%) are emitted during the de-excitation. Vacancies in the electron shells of ^{125}I are created because of the electron capture and conversion electron emission. Characteristic X-ray photons are emitted every decay (140%) with a mean energy of 28 keV. Energetic Auger electrons are also emitted instead of X-ray emission [14]. All electrons are absorbed in the glass in which the iodine solution is kept. Consequently the radiation reaching the experimental set-up consists of two discrete energies; one at 28 keV and one at 35 keV. At the time of the exposure, the 11:th of January 1995, the strength of the source was 3.2 MBq. Two IP's were exposed, IP:1 with a short distance from the source (20 cm) and IP:2 with a longer distance (60 cm). Since the intensity is proportional to $1/r^2$ were r is the distance from the source, the incoming intensity of IP:1 was nine times larger than the incoming intensity of IP:2. Each IP was divided into nine fields which were exposed with different exposure times varying from 0 to 130 minutes (see Fig. 4-3). The experimental set-up is shown in Fig. 4-4.

IP:1

0	15	42
5	21	62
10	33	129

IP:2

1	2	10	60
0	5	30	120

Figure 4-3. The IP:s are exposed with different exposure times in minutes.

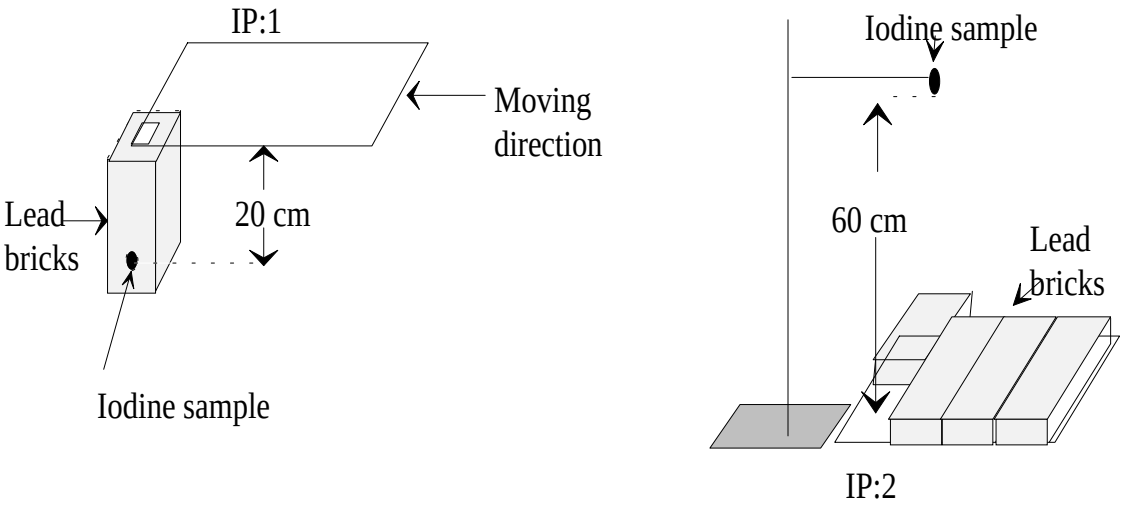

Figure 4-4. IP:1. The iodine sample is covered by four 50 mm thick lead bricks forming an X-ray collimator. On the top of the lead bricks there is a rectangular hole where the IP can be exposed. The nine fields which IP:1 is divided in are exposed with different exposure times by moving the IP over the lead bricks. IP:2. The IP is covered by four 50 mm thick lead bricks except one field which is exposed with the iodine sample. The eight fields of IP:2 are exposed with different exposure times by moving the lead bricks.

4.2.2 Results and conclusions

The relation between the number of photons reaching the IP and the blackness of the IP is investigated. It is also desirable to see if the spread of the pixel values fits a Gaussian distribution so the statistical error in pixel value (σ_{QLbmp}) can be estimated.

$$Gaussian\ Distribution = e^{-\frac{(QL_{bmp}-QL_{bmp0})^2}{(2\cdot\sigma)^2}} \quad (6)$$

QL_{bmp} = the pixel value

QL_{bmp0} = the pixel value with highest intensity representing the average blackness

σ= the standard deviation of the pixel values

It is known from statistic theory [9] that a sum of stochastic variables is approximately a normal distribution, if the number of components in the sum, n, is large enough. N is in this case the number of photons reaching the IP which is proportional to the exposure time. The standard deviation is proportional to $\sqrt{n}$ and the pixel value, QL_{bmp0}, is proportional to n. In this case IP:1 is exposed with nine times higher dose than IP:2. The IP:s have nine and eight different fields respectively, with increasing exposure times, i.e. increasing doses. The number

of photons reaching the IP is proportional to the incoming intensity, i.e. the dose, and the PSL value. Each field of the IP represents a certain dose. With software developed for this purpose (see Sect. 6) the pixel values from each field are transformed into PSL values and subsequently averaged. The PSL values are plotted as a function of exposure times (Fig. 4-5).

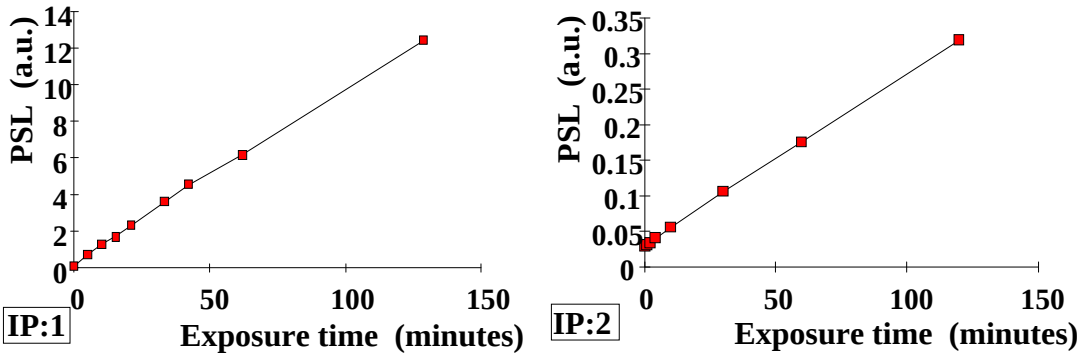

Figure 4-5. PSL value as a function of exposure time. IP:1: Distance to sample: 20 cm. IP:2: Distance to sample: 60 cm.

The relation is linear in the whole range as expected. Equal areas from each field are analysed and the intensities of the pixel values, i.e. the sum of pixels with the same value, are plotted as a function of the pixel values (0 - 255), to see the spread in pixel values (Fig. 4-6). The distribution is well fitted to a normal distribution. A least square fit of the pixel values to a normal distribution is made for each of the nine/eight fields in each IP. The relation σ_{PSL} (width) to the square root of the exposure time is plotted in Fig. 4-7. As expected it is a linear function. The σ_{PSL} increases as the exposure time increases. We now have a relation between the standard deviation and the dose that we can use in future measurements (see Sect. 7.2).

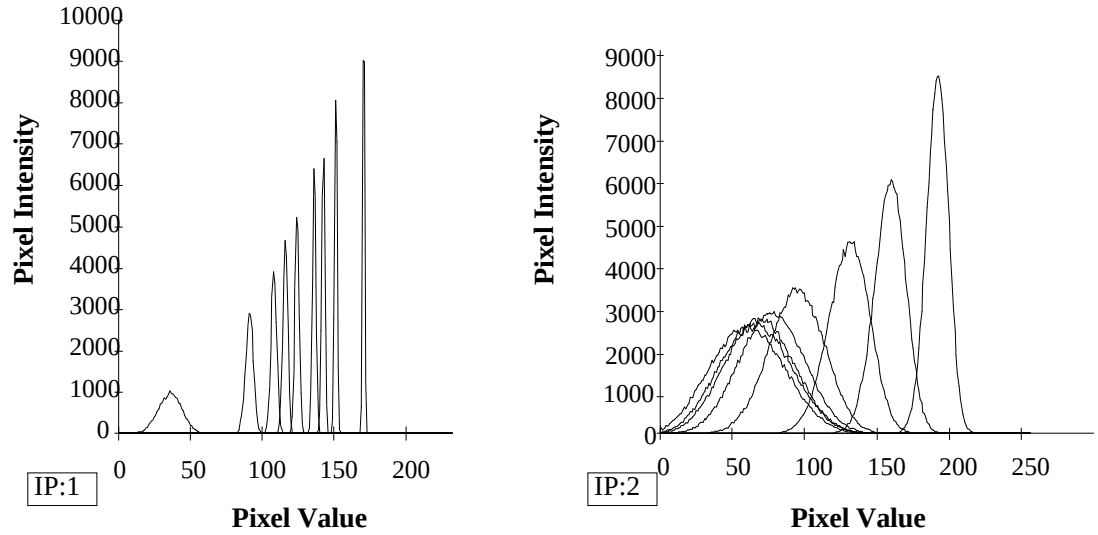

Figure 4-6. Pixel intensity as a function of pixel value. IP:1 is exposed with a dose that is nine times bigger than the exposure dose of IP:2. Each curve in one diagram correspond to a certain exposure time. When the exposure time increases the pixelvalue increases and the curve gets higher and thinner. i.e. the relative error, σ_{QLbmp}/QL_{bmp0} , decreases. Hence, the curves from IP:1 are much thinner than the curves from IP:2 since the exposure is nine times bigger.

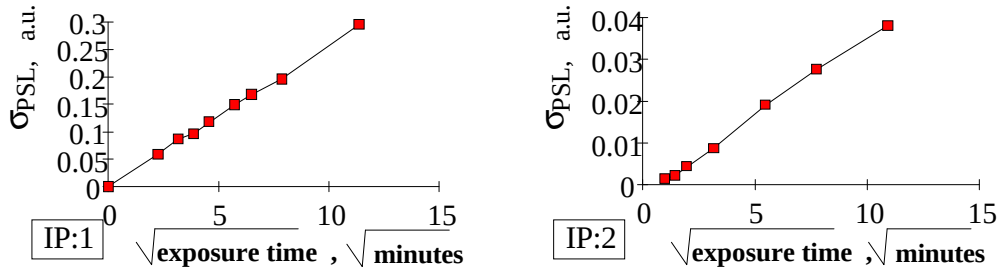

Figure 4-7. σ_{PSL} as a function of √exposure time.

4.2.3 Image plate sensitivity

The blackness of the IP depends on how much energy it absorbs. As known from the theory (Sect. 2) the absorption curve is a function of energy and atomic number. The elements in the IP are mainly Ba, Br, I and F. Depending on their relative contents the total absorption curve of the IP looks different (Fig. 4-9). The absorption (A) is

$$A = I_0(1 - e^{\mu_{IP} \cdot x}) \quad (7)$$

where μ_{IP} is the total absorption coefficient of the IP and x is the thickness.

$$\mu_{IP} = a \cdot \mu_{Ba} + b \cdot \mu_{Br} + c \cdot \mu_F + d \cdot \mu_I \quad (8)$$

where a, b, c, and d are the partial fractions of the elements. Generally speaking the absorption is larger for low energies than for high. The absorption as a function of energy for some different compositions of Ba, Br, F and I are shown in Fig. 4-8.

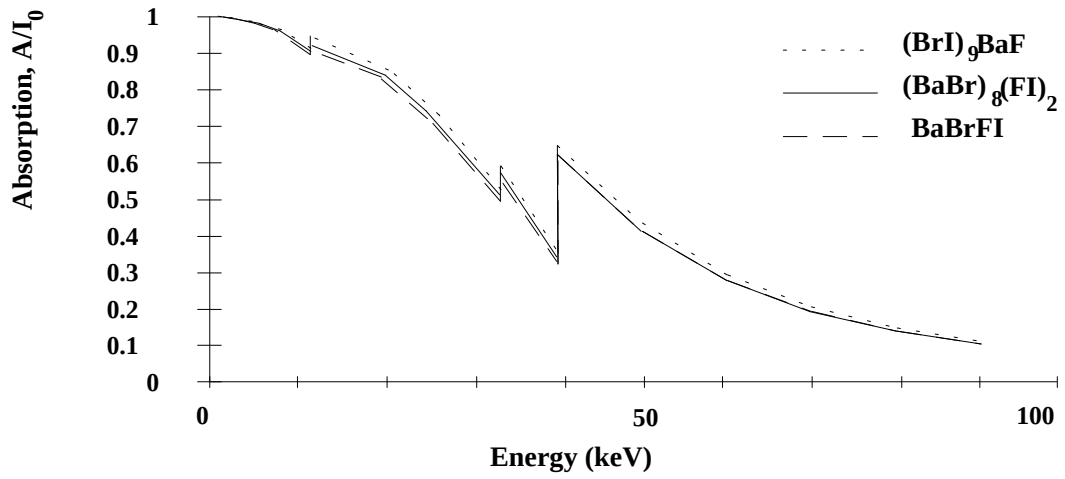

Figure 4-8. The absorption of X-rays in an Image Plate with different compositions of Ba, Br, I and F.

5. Filters

Filters of different elements are used in this work to examine the differential absorption through them. We would like to use all elements for fabrication of filters but for different reasons, such as prices and chemical and physical properties, it is difficult.

5.1 Possible filters

Which elements should be chosen? It depends on which energy range that is examined. It is possible (theoretically) to find naturally abundant elements to cover an energy range up to 116 keV (i.e. z = 92) (see Table 5-1). The resolution should be ≈1 keV for low energies and 1.5 - 2 keV for high energies (>50 keV) choosing all elements. Unfortunately this is not possible. Some of the elements are very expensive and quite difficult to obtain, and some of them have chemical and physical properties which make it impossible to use them for this purpose. For example in the energy interval from 50 to 70 keV, where tantalum has its characteristic K-lines, there are eleven elements with atomic number from 64 to 74. Of those lutetium is not possible to use because of its radioactivity which affects the IP. The other elements are useful but the prices vary. As said before the absorption coefficient depends on the atomic number and the energy. It increases as z increase, and decreases as the energy increases. The higher energy range that is examined the heavier elements should be chosen.

An alternative to pure elements is to make solutions of metal salts with matched concentrations. Working in the energy range of the characteristic lines from the laser produced plasmas, i.e. hard X-rays, the absorption contribution of the metal compound in the salt dominate over the absorption in the lighter elements (N, O, Cl etc.) since the metal has a high atomic number. Consider the absorption in the metal salt $Pb(NO_3)_2$. The absorption in Pb is 17 times higher than the absorption in $(NO_3)_2$ at 60 keV.

Atomic number	25	26	27	28	29	30		83	84	85	86	87	88	
Element	Mn	Fe	Co	Ni	Cu	Zn		Bi	Po	At	Rn	Fr	Ra	
K-edge (keV)	6.5	7.1	7.7	8.3	9.0	9.7		90.5	93.1	95.7	98.4	101.1	103.9	

Table 5-1. Some elements with their K-edges and atomic number.

5.2 Solutions

The advantage of using solutions as filters is that they are easier to mix in different concentrations for the matching of filters. This is important since there is an error contribution from not having exactly matched filters (see Sect. 7). On the other hand it is difficult to examine a spectrum in a low-energy region since the absorption of X-rays in the light elements of the salt is relatively large. A diagram of the absorption coefficients of the different compounds in the metal salts at various energies is shown in Fig. 5-1.

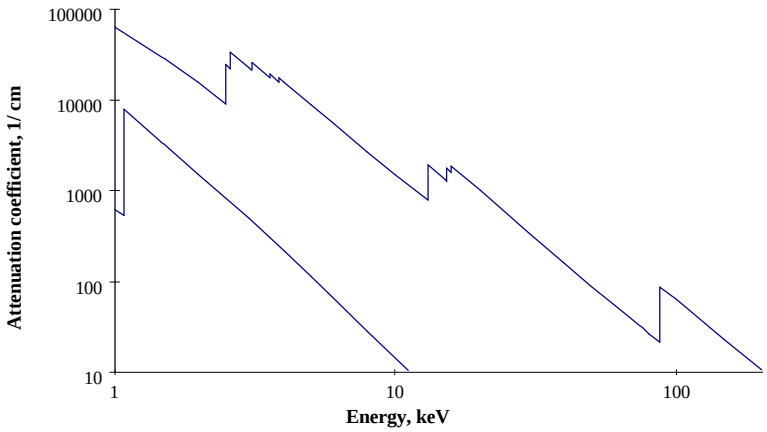

Figure 5-1. Absorption coefficient as a function of energy for lead and sodium. At the energy range 10 to 100 keV the attenuation coefficient of lead is ≈100 times higher than that of sodium.

5.3 Foils

The most prominent advantage of using foils as filters is that it is only one element that absorbs X-rays. It is then possible to examine even the Bremsstrahlung spectrum (at low energies) which is difficult with solutions. The problem with foils is how to make exactly fitting thickness, how to make a foil which does not vary too much in thickness and how to measure the foil thickness with an error that is not too large.

5.3.1 Treating foils

The optimal transmission for examinations of the characteristic lines in tantalum is 50% in this energy region (see Sect 7). This leads to thickness from 0.04 mm (Pb) to 0.13 mm (Gd). The relative error contribution in thickness from the lead foil gets big since the foil is rather thin compared to the gadolinium foil. It is necessary to have an accurate thickness, especially for the heavy element foils since they are thinner. The foils can be rolled under a variable pressure. This is the method used in this work to treat the foils. The higher the pressure is during the rolling, the thinner the foils will be. Unfortunately, the thickness varies over the surface. It is also difficult to get exactly the thickness wanted. The variation, Δs, is 2 - 4 microns measured with a micrometer. This is a variation of 10 % over the lead surface. Foils with a specific thickness that varies less than 2 % over the surface are commercially available (Goodfellow Cambridge Ltd).

5.3.2 Measuring foil thickness

There are several ways of measuring the foil thickness. Three methods are described in this section.

a) Weighing the foils and calculate the thickness.

Punching out small circles with the same diameter it is quite easy to weigh the foils and by the density calculate the thickness.

$$x = \frac{m}{A \cdot \rho} = \frac{m}{\pi \cdot r^2 \cdot \rho} \tag{9}$$

x = thickness of the foil, m = mass of the foil, A = area of the foil, r = radius of the foil circle, ρ = the density of the foil

The error, Δx, in this method comes principally from the radius error, Δr, during the punching. The balance used for weighing the foils is very accurate ($\Delta m = 5 \cdot 10^{-6}$g , $\Delta m/m$ <0.1%).

$$\frac{\Delta x}{x} = \frac{2 \cdot \Delta r}{r} \qquad (10)$$

b) Micrometer

The micrometer used here is a very sensitive instrument from Mitutoyo showed in Fig. 5-2. A small spherical bullet is mounted on a planar glass plate. The foil is put between the bullet and the measuring head. The thickness is directly read on the meter scale. The error in thickness measurements is 2 microns with this instrument.

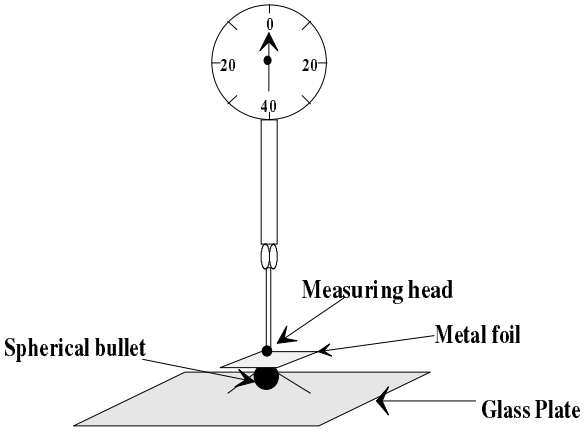

Figure 5-2. A figure of the micrometer used.

c) Exposure of filters with a mono-energetic source.

It should be accurate to measure the transmission of X-rays from a mono-energetic source through the filters. There are several aspects to consider which are described in detail in Sect. 7-2. The measurement is described in Sect. 7-3.

6. Computer programme

A computer programme is written to simplify the spectral analysis made from the blackness of the filters in the bit map pictures. Looking at the picture in bit map format with a graphical programme called Publishers Paintbrush, it is seen that the pixel values (0-255), which represent the blackness, vary over the filter surface. The programme reads the bit map picture and calculates the averaged PSL value, with subtracted PSL_{offset} value, for each filter. The result is stored in an output file. There after it is easy to subtract the PSL values pair wise, which represents the integrated intensity in a specific energy interval. The integrated intensities are subsequently plotted as a histogram, with box widths corresponding to the energy interval. In the future the programme should of course do the subtraction and draw the preliminary spectra. Inputs for the programme are information about the IP such as scanning parameters (latitude and sensitivity), maximum and minimum pixel value from the file conversion, co-ordinates of the filters and output filename. The co-ordinates are taken from the digital picture in Publishers Paintbrush. The programme is described in Appendix A.

The programme is written in Borland Pascal 7.0 for a Windows environment. The programme uses a read module that reads a bit map file and puts the numerical values in a matrix. This module is written by Mattias Grätz. The flow chart that describes the algorithm is shown below.

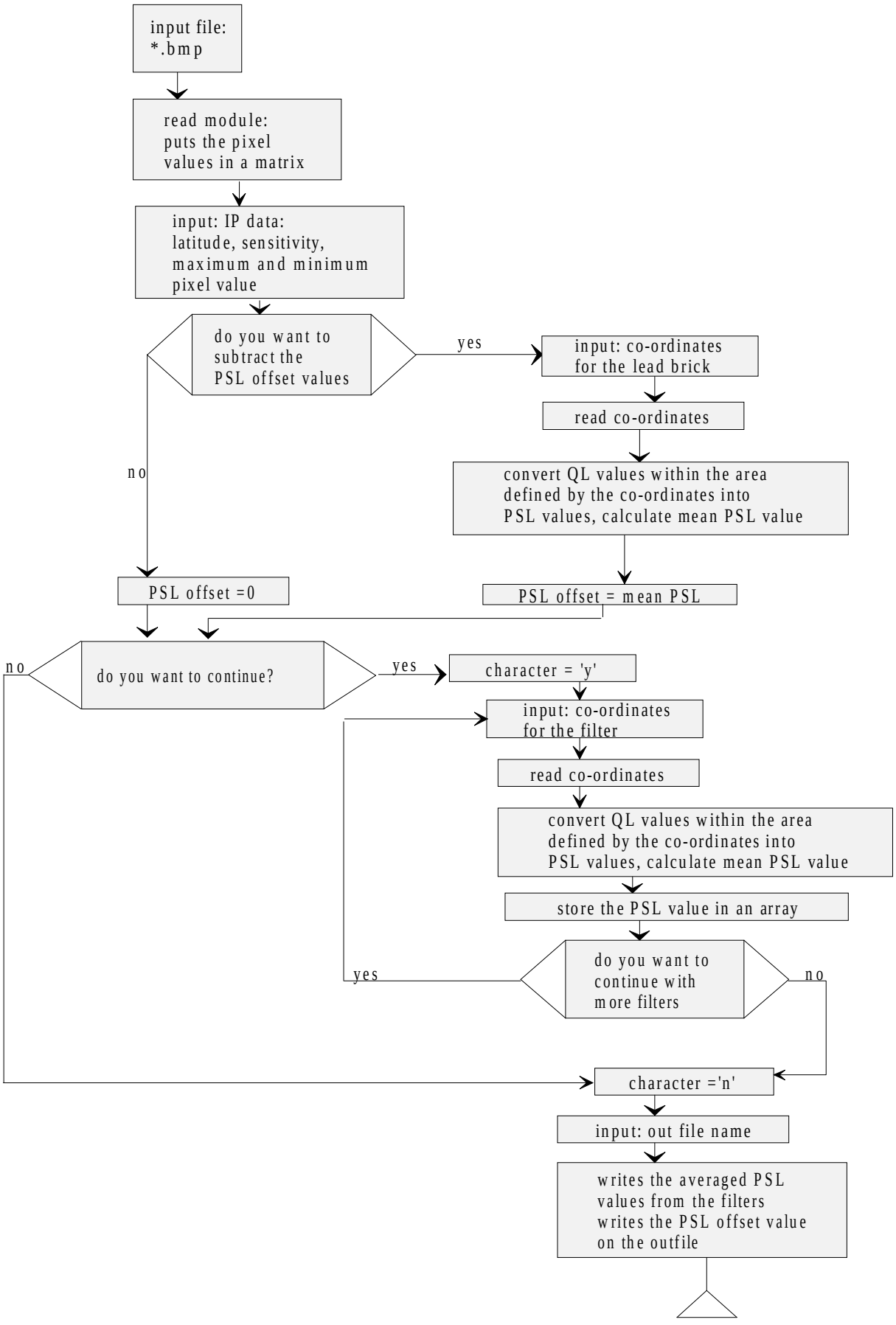

Figure 6-1. Flow chart for the programme.

7. Preliminary spectral measurements

Three different radiation sources were used to examine the spectral distribution by exposing the IP through a filter set:

- Mono-energetic iodine source
- Laser-produced plasmas
- X-ray tube

7.1 Error analysis

Different errors affect the total spectral result. An example is the error coming from badly matched filters. It means that the filters are not perfectly matched, i.e. the transmission through the filters before their K-edges is not the same. The differences in transmitted intensity before and after the K-edges are not zero when we do the subtraction of the transmission of two filters (Fig. 7-1).

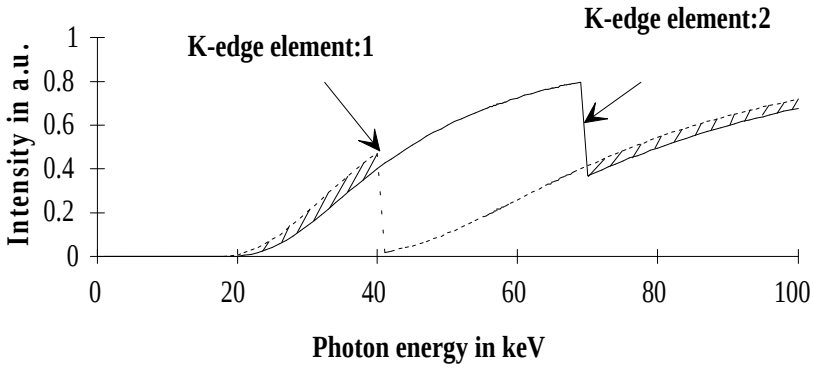

Figure 7-1 The transmission spectra of two elements. The thickness are not perfectly matched i.e. the curves before and after the K-edges do not overlap. There are small areas (marked ///) which contribute to the error.

7.1.1 Transmission errors

The transmission errors depend on different factors as shown in Fig 7-2. Two of those factors which probably are the most important are analysed.

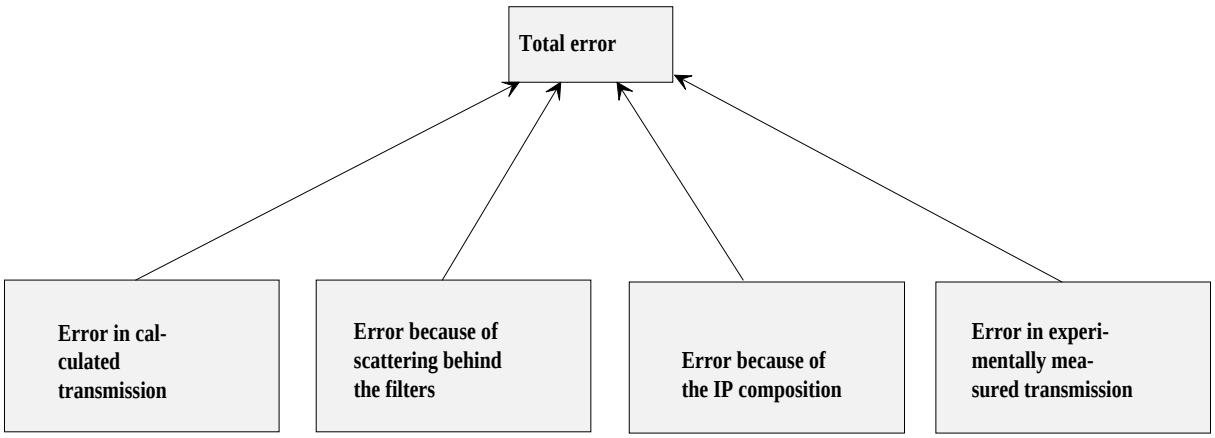

Figure 7-2.

7.1.1.1 Error in calculated transmission

It is known from Beer-Lambert's law that the transmission (*T*) of radiation through a medium is given by

$$T = e^{-\mu \cdot x}, \tag{11}$$

where μ is the attenuation coefficient (1/cm) and x is the thickness (cm) of the medium.

The error in thickness measurements , Δx, is about 2 - 4 μm with the micrometer that was used (see Sect. 5.4.2.b). The error in absorption coefficient, $\Delta\mu$, is small compared to the error in thickness measurements [10].

The relative error in transmission because of errors in thickness measurements is in the first order approximation

$$\frac{\Delta T_1}{T} = -\mu \cdot \Delta x \tag{12}$$

The relative error in transmission because of errors in μ

$$\frac{\Delta T_2}{T} = -x \cdot \Delta\mu \tag{13}$$

If we summarise those errors we get

$$\frac{\Delta T}{T} = \sqrt{(\frac{\Delta T_1}{T})^2 + (\frac{\Delta T_2}{T})^2} \tag{14}$$

$$\text{if } \frac{\Delta T_1}{T} >> \frac{\Delta T_2}{T} \text{ then } \frac{\Delta T}{T} = -\mu \cdot \Delta x \tag{15}$$

7.1.1.2 Error in the experimentally measured transmission

The value that we get from the blackness of the IP is proportional to the incoming intensity and the number of photons that reach the IP (see Sect 4.1).

The experimentally measured transmission is

$$T_{psl} = \frac{I}{I_0} = \frac{PSL_{filter} - PSL_{offset}}{PSL_{bkg} - PSL_{offset}}, \tag{16}$$

where

PSL_{filter} is the *PSL* value from the IP after filtration,

PSL_{bkg} is the PSL value from the background on the IP,

PSL_{offset} is the offset PSL value (see Sect. 4) coming from the IP exposed only with background radiation, that is the value under a 50 mm thick lead brick.

Equation 1 gives

$T_{psl} = 10^{\frac{l \cdot (QL - QL_{bkg})}{N}}$ (see Sect. 4)

Since *l* and *N* are constants the error depends on the *QL* values.

There are two types of errors in *QL* values:

- Quantisation error
- Standard deviation of *QL* values because of a Gaussian distribution

Quantisation error

The *QL* values vary from 0 to 1023. They are converted with a computer programme to pixel values that vary from 0 to 255. (see Sect. 4). The quantisation error in pixel value is $\pm\frac{0.5}{256}$ because of the 256 steps (see Fig 7-3). The error, ΔQL, is

$$\Delta QL = \frac{QL_{\max} - QL_{\min}}{512} \tag{17}$$

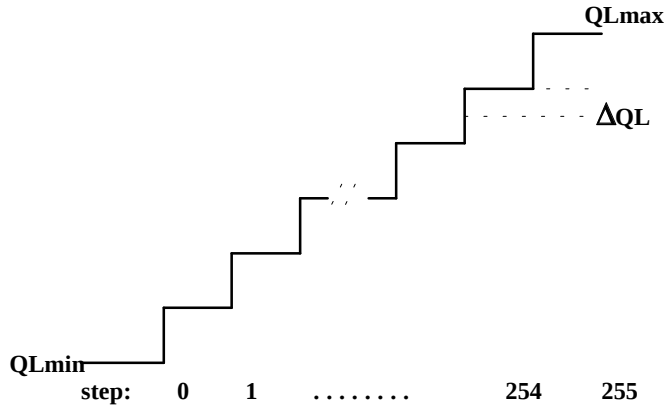

Figure 7-3. Illustration of the quantisation error.

The relative transmission error becomes

$$\frac{\Delta T_{psl1}}{T_{psl}} = \frac{l \cdot \ln 10 \cdot \sqrt{\Delta QL^2 + \Delta QL_{bkg}{}^2}}{N} = \frac{l \cdot \ln 10 \cdot \sqrt{2} \cdot \Delta QL}{N}, \tag{18}$$

$(\Delta QL = \Delta QL_{bkg})$

which is constant.

Standard deviation of *QL* values

It is known from section 4 that an area of a homogeneous blackness gives an ensemble of QL values which look like a Gaussian distribution if we plot the number of points with a certain pixel value as a function of that pixel value (See Eq. 6).

The average blackness is identified by QL_{bmp0} which is the pixel value that most of the points have (see Fig 2.2.3). The error, which is the standard deviation of the pixel values σ_{QLbmp}, comes from the width of the Gaussian curve. The probability that the pixel value lies in an interval of $\pm\sigma$ is 68%, and the probability that the same value lies in an interval of $\pm 2\sigma$ is 95 % for a Gaussian distribution (σ= standard deviation) [9]. Using the same exposure time for all filters we get different Gaussian curves for different transmissions where $\sigma_{psl} = const \cdot \sqrt{T_{psl}}$, since σ_{psl} is proportional to $\sqrt{n}$, where n is the number of photons (see Sect. 4) and n is proportional to the transmission, T.

The relation between σ_{QLbmp} and σ_{PSL} is

$$\sigma_{psl} = const \cdot PSL \cdot \sigma_{QLbmp} = const \cdot \ln(10) \cdot \frac{l}{N} \cdot 10^{l(\frac{pix \cdot (QL_{\max} - QL_{\min})}{255 \cdot N} + \frac{QL_{\min}}{N} - \frac{1}{2})} \cdot \sigma_{QLbmp}$$

The relative transmission error becomes

$$\frac{\Delta T_{psl2}}{T_{psl}} = \frac{l \cdot \ln 10 \cdot (QL_{\max} - QL_{\min}) \cdot \sqrt{\sigma_{bkg}{}^2 + \sigma_{filter}{}^2}}{N \cdot 256} \quad , \qquad (19)$$

where σ_{bkg} is the standard deviation from the background pixel value and σ_{filter} is the standard deviation from the filter pixel value.

The sum of the relative errors in T_{psl} becomes:

$$\frac{\Delta T_{psl}}{T_{psl}} = \frac{\sqrt{\Delta T_{psl1}{}^2 + \Delta T_{psl2}{}^2}}{T_{psl}} = \frac{l \cdot \ln 10 \cdot (QL\max - QL\min) \cdot \sqrt{\sigma_{filter}{}^2 + \sigma_{bkg}{}^2 + 0.5}}{N \cdot 256} \qquad (20)$$

using that $\sigma_{psl} = C \cdot \sqrt{T_{psl}}$

$$\frac{\Delta T_{psl}}{T_{psl}} = \sqrt{(\frac{\sigma_{psl}}{T_{psl}})^2 + C^2} = C_1 \cdot \sqrt{\frac{1}{T_{psl}} + C_2{}^2} \qquad (21)$$

As we can see in Fig. 7-4 the error becomes very large for low transmissions.

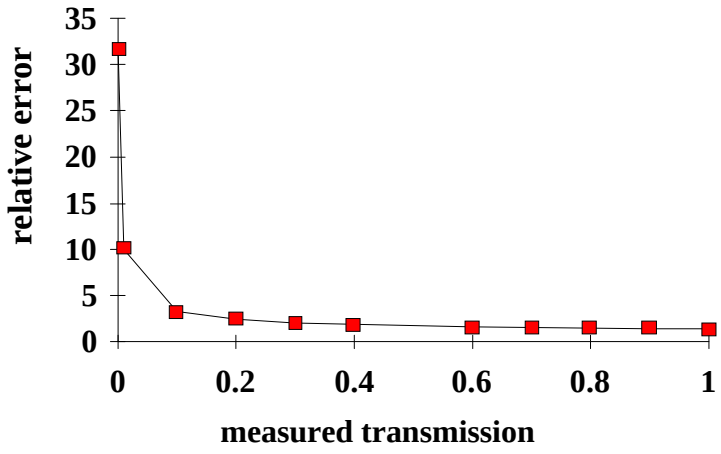

Figure 7-4. The relative error in transmission is plotted as a function of measured transmission

7.1.2 The total error

If we summarise the error analysis above (and neglecting scattering errors and IP composition errors) we get

$$\frac{\Delta T}{T} = \sqrt{(\frac{\Delta T_{psl}}{T_{psl}})^2 + (\frac{\Delta T_{cal}}{T_{cal}})^2} = \sqrt{C_2{}^2 (\frac{1}{T_{psl}} + C_1) + (\mu \cdot \Delta x)^2)} \qquad (22)$$

The relative error is a function of transmission, energy and atomic number since, μ is a function of energy and atomic number (see Sect. 2.3).

7.2 Iodine Exposures

A sample of radioactive ^{125}I was used and an IP was exposed through a set of foils with varying thickness and atomic number (Z) to verify the method and to measure the foil thickness. The experimentally measured transmission was then compared with the calculated transmission. It was also calculated how the IP composition affected the experimentally measured transmission.

7.2.1 Experimental set-up

The iodine solution contained in a small glass bottle was placed 60 cm over the IP and the foils lied directly on the IP (Fig. 7-5).

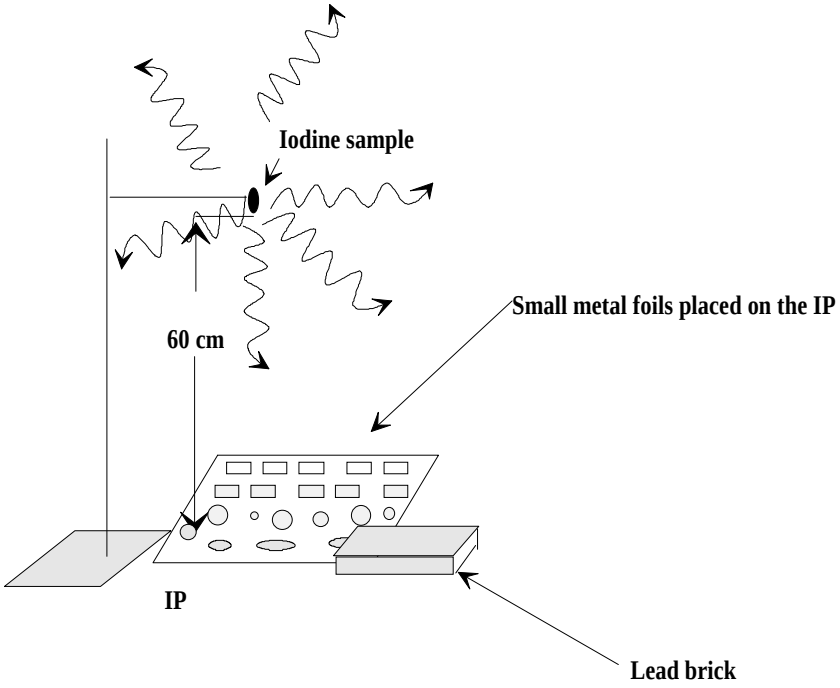

Figure 7-5. Experimental set-up

The strength of the sample was 4 MBq at the time for the experiment and the exposure time was 4 hours 30 min. The thickness of the elements was measured with a micrometer (Sect. 5.4.2.b).

7.2.2 Results and conclusions

After exposure, scanning the IP and converting the img format to bmp format the picture was analysed. The PSL values from each filter and the surrounding background was averaged and then the background radiation PSL value was subtracted and saved in a new file with help of the software. A Gaussian curve was adapted to the pixel values of each filter to determine the standard deviation, σ_{QLbmp}, of the pixel values and the standard deviation of the PSL values, σ_{PSL} (Sect. 4). The transmission and the square root of the transmission was plotted against σ_{PSL} which verifies that the error is proportional to the square root of the number of photons

reaching the IP (Fig. 7-6). The experimentally measured transmission was plotted to the calculated transmission with error bars (Sect. 7.2) (Fig. 7-7).

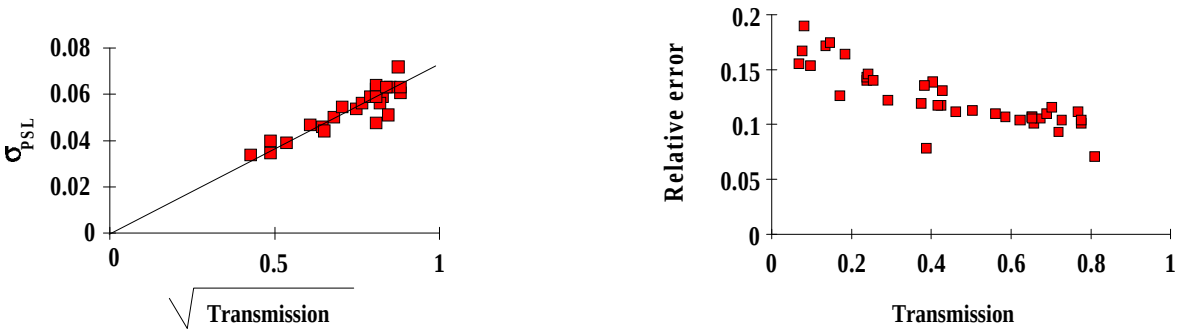

Figure 7-6. σ_{PSL} as a function of $\sqrt{T}$ (a) and σ_{PSL}/T as a function of the transmission T (b). Comparing diagram (b) with Fig. 7-4 it is seen that this experimental curve agrees with the theory.

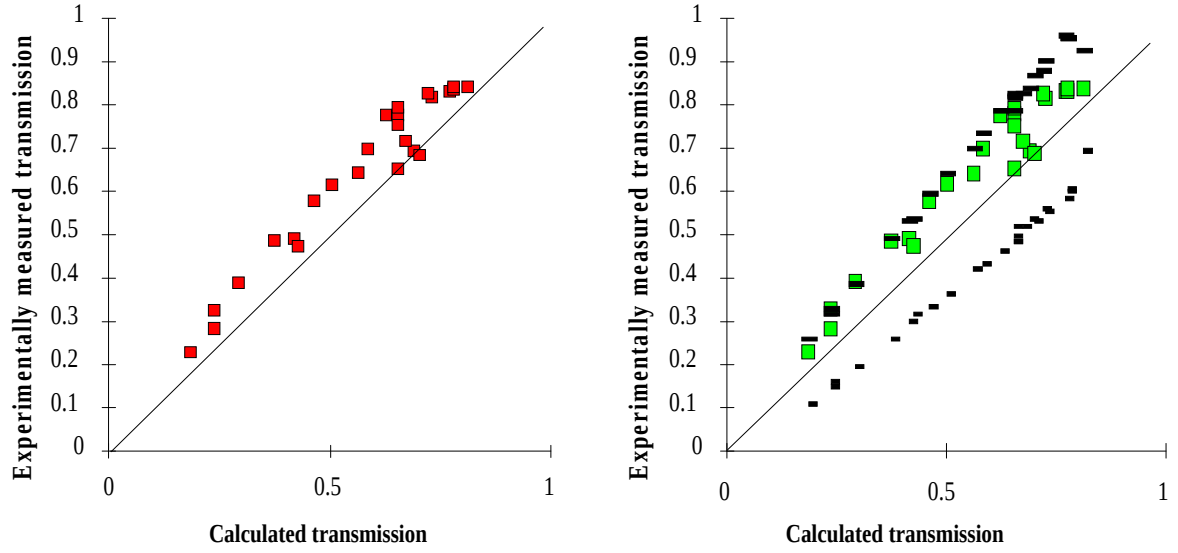

Figure 7-7. Experimentally measured transmission as a function of calculated transmission (marked with squares) with and without errorbars (marked with -). The strait line is a help line which denotes the measured transmission = the calculated transmission.

As seen in the figure all transmission values lie between the error bars. Since the filters were not perfectly matched in thickness (because of the treating method of the metal foils in Sect. 5.4.1) it was difficult to use the subtraction of filters in this case to find the peaks in the iodine source. Different discrete single line spectra were simulated to see if their calculated transmission values lied between the error bars from the iodine transmission diagram (Fig. 7-8). As seen in the figure, the points from the simulated spectra lie outside the error bars. That means that the simulated spectrum is not the correct spectrum. It is possible to find the most probable spectrum by repeating this action and maybe do an iterative algorithm for the purpose. This method is of course hard to use for a continuous spectra but it shows that it is possible to use the IP for quantitative measurements.

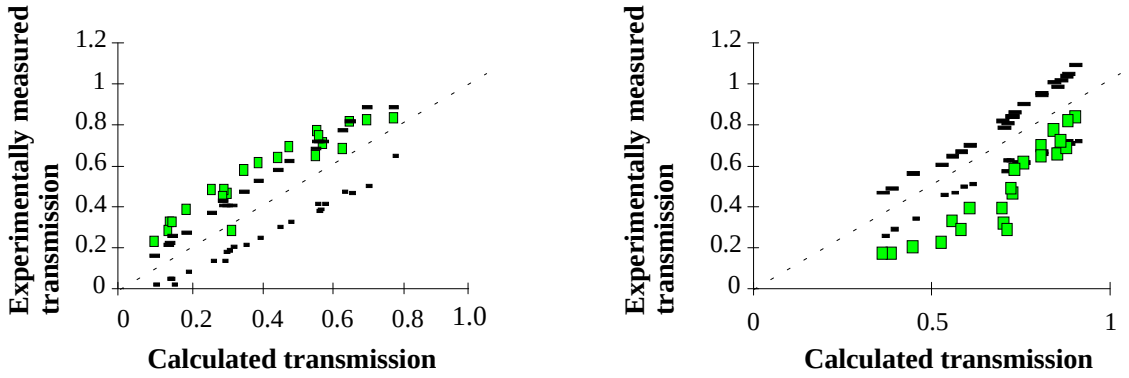

Figure 7-8. The calculated transmission from two simulated discrete single line spectra; one at 28 keV and one at 40 keV, were put in the transmission diagram from the iodine exposure. This means that the measured transmission from the iodine exposure was plotted as a function of calculated transmission from the simulated spectra. Notice that almost all the values lie outside the error bars. If the simulated spectrum was the true spectrum, the calculated transmission values should have laid between the error bars.

7.3 Laser produced plasma

7.3.1 Laser system and experimental set-up

The laser system used in this experiment was a terawatt laser system based on chirped pulse amplification in titanium-doped sapphire. The laser is tuneable between 760 nm (1.63 eV) and 840 nm (1.47 eV) and operates at 10 Hz. The pulse length is 150 fs and the pulse energy is up to 220 mJ corresponding to a peak power of 1.5 TW [11]. See Fig. 7-9.

The generation of X-rays comes from focusing the terawatt laser beam on a solid target placed in a vacuum chamber. The focal intensity is near 10^{18} W/cm^2. The pressure in the chamber is 20 Torr to prevent the sputtering of target material on the optics. A thin glass pellicle is inserted between the mirror and the target to protect the mirror. The laser beam enters the chamber through a glass window and is focused by an off-axis gold-coated parabolic mirror with a low f number. The focused beam reaches the target which is a tantalum or a gadolinium foil glued on rotating steel disks. Every laser pulse creates a plasma and makes a small hole in the target material. The rotation makes sure that every new laser shot hits a fresh area on the target. The X-rays pass through a plastic window, with low absorption for hard X-rays, out of the chamber. An aluminium filter is placed outside the window to absorb the low energetic X-rays. The remaining X-rays reach the IP after passing through the filter system. It is possible to have different spectra by changing the target material. The Bremstrahlung spectrum is expected to be approximately the same for different elements but the characteristic lines are unique for each element [1,13]. The set-up is shown in Fig. 7-9 and 7-10.

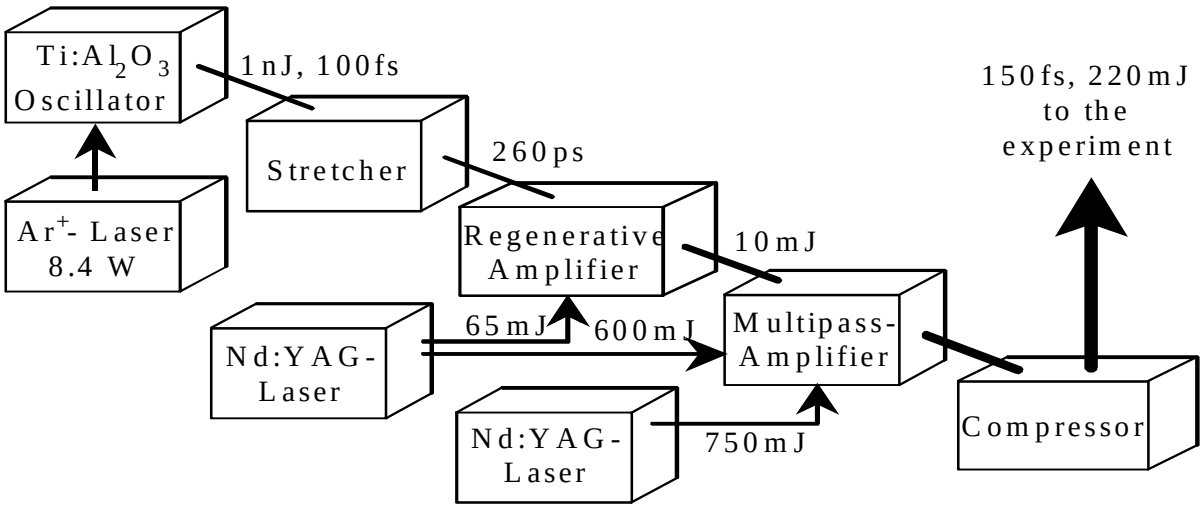

Figure 7-9. The terawatt laser system.

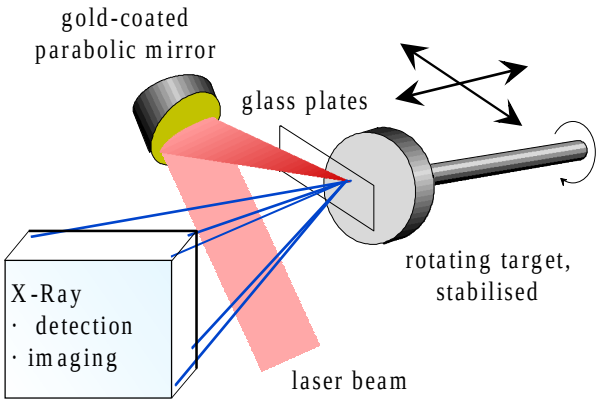

Figure 7-10. The laser beam is focused onto the target and a plasma is created which generates X-rays used for exposure of the IP through the filters.

7.3.2 Experiment and conclusions

A set of solutions are used for the filter system instead of metal foils. It is easier to make matching concentrations than matching foil thickness. The absorption in the light element of the salt is fairly low in the energy region of the characteristic lines of tantalum and gadolinium. The error in filter thickness, $\Delta x/x$ (Sect. 7.1.1), coming from the error in concentration, c, is $\Delta x/x = \Delta v/v$ since

$$c = \frac{x \cdot \rho}{d \cdot M} = \frac{m}{M \cdot v} \rightarrow x = \frac{m \cdot d}{v \cdot \rho}$$

$$\frac{\Delta x}{x} = \sqrt{(\frac{\Delta m}{m})^2 + (\frac{\Delta v}{v})^2} \qquad \frac{\Delta m}{m} << \frac{\Delta v}{v}$$

where m is the mass of the metal salt, M is the molar mass, v is the water volume and d is the thickness of the TCA, which is 5 mm. Metal salt compounds are found for energy intervals of

≈10 keV to cover an energy range from 40 to 88 keV. Five solutions are used with K-edges at 40, 50, 61, 69 and 88 keV (see Table 7-1).

Metal- salt:	K-edge of metal compound (keV):
$Ce(NO_3)_3 \cdot 6H_2O$	40
$Gd(NO_3)_3 \cdot 6H_2O$	50
$Yb(NO_3)_3 \cdot 5H_2O$	61
$H_3(P(W_3O_{10})_4) \cdot XH_2O$	69.5
$Pb(NO_3)_3$	88

Table 7-1. Solutions in TCA:s.

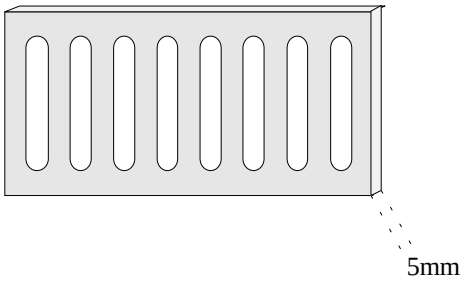

Figure 7-11. A 5 mm thick TCA.

The solutions are put in Test Cell Arrays, TCA:s, [15] which are made of Plexiglas (Fig. 7-11). There are eight oblong holes in a TCA. The TCA has a uniform thickness of 5 mm. Two TCA:s are filled with solutions with matched concentrations so that they can be directly subtracted from each other (TCA:1 minus TCA:2). That means that the transmission is the same before and after the K-edges for each pair of solutions. The first four cells in both TCA:s are matched so that all solutions have the same transmission before the lowest K-edge and after the highest K-edge. The second four cells are matched pair wise (TCA:1, cell 5 matched with TCA:2, cell 5) (Fig. 7-12).

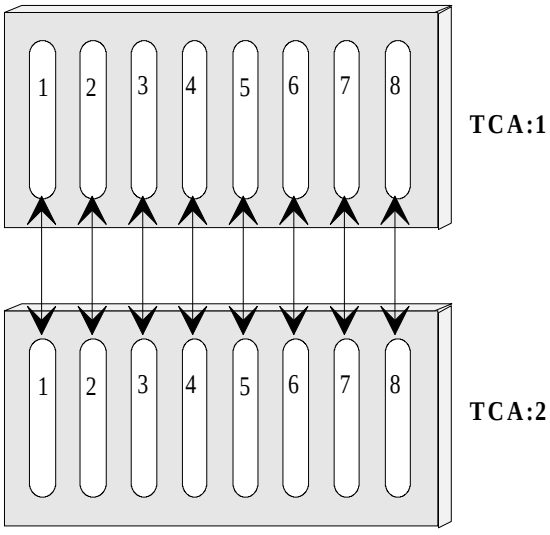

Figure 7-12. The cells are matched pair wise. Each pair of cells connected with an arrow have matched concentrations.

Test cell:	Substance:	Conc(molar)	Trans at 40 kev	Trans at 50 kev	Trans at 60 kev	Trans at 90 kev
1	$Pb(NO_3)_3$	0.88	30	51	66	54
2	$H_3(P(W_3O_{10})_4)\cdot XH_2O$	1.26	30	51	65	51
3	$Yb(NO_3)_3\cdot 5H_2O$	1.53	30	51	65	50
4	$Gd(NO_3)_3\cdot 6H_2O$	2.21	30	51	12	49
5	$Pb(NO_3)_3$	1.3			50	
6	$H_3(P(W_3O_{10})_4)\cdot XH_2O$	2			50	
7	$Yb(NO_3)_3\cdot 5H_2O$	1.61	29	50	65	49
8	$Gd(NO_3)_3\cdot 6H_2O$	1.3	50			
TCA: A_3						
Test cell:	Substance	Conc(molar)	Trans at 40 kev	Trans at 50 kev	Trans at 60 kev	Trans at 90 kev
1	$H_3(P(W_3O_{10})_4)\cdot XH_2O$	1.26	30	51	65	50
2	$Yb(NO_3)_3\cdot 5H_2O$	1.53	30	51	65	50
3	$Gd(NO_3)_3\cdot 6H_2O$	2.21	30	51	12	49
4	$Ce(NO_3)_3\cdot 6H_2O$	3.2	30	3	12	49
5	$H_3(P(W_3O_{10})_4)\cdot XH_2O$	2			50	
6	$Yb(NO_3)_3\cdot 5H_2O$	2.5			50	
7	$Gd(NO_3)_3\cdot 6H_2O$	2.21	30	51	12	
8	$Ce(NO_3)_3\cdot 6H_2O$	1.8	50			

Table 7-2. The transmission in % for different compounds, concentrations and energies.

The concentrations and transmissions of the solutions in the TCA:s are shown in Table 7-2. Two IP:s were exposed, one with a tantalum target and one with gadolinium target. The first IP was divided into four fields and the second IP was divided into two fields, each field exposed with different filtering of the X-rays before reaching the IP and the filter system (see Table 7-3). The fields which were unexposed were protected with 50 mm thick lead bricks.

	Field 1:	Field 2:	Field 3:	Field 4:
IP:1, Ta target	Al filter	Gd filter	Ta filter	No filter
IP:2, Gd target	Al filter	No filter		

Table 7-3. The different fields in the two IP:s.

The digital images from the IP:s are shown in Fig. 7-13. Looking directly at the two digital images in Fig. 7-13 it is almost impossible to see any differences between them, but after subtracting the two images, the differences show up (Fig. 7-14). The darkest pixels represent the lowest exposure value and the lightest pixels represent the highest exposure value. After subtraction, the darkest field represent the smallest difference in pixel value and the lightest field represent the largest difference in pixel value. The lighter the field is, the higher the integrated intensity is in this energy interval determined by the K-edges of the two subtracted elements. With this in mind, it is possible just by looking at the differentiated picture to identify which picture that belongs to a certain filter and target shown in Table 7-3 (see Fig. 7-15 - 7-18). For example, comparing the two differentiated pictures from the tantalum target with a gadolinium filter and with no filter (Fig. 7-15 and Fig. 7-16) it is seen that the cell representing the energy interval 50-60 keV is darker in the image which is filtered with gadolinium than the unfiltered one. Dark means low intensity in this interval and can be explained by the K-edge of gadolinium which has its position at 50 keV. This means that the transmission just before 50 keV is large and after 50 keV is low. The images are transformed into histograms, by transforming the pixel values, which gives a rough estimation of the spectral distribution of each case. The histograms are then compared with a theoretical spectrum (Fig 7-15 -7-18).

The conclusions from this experiment is that it is possible to have a rough estimation of the spectrum from X-rays coming from a laser-produced plasma by looking at the differential absorption through a filter system of solutions with matched concentrations. The resolution gets higher and the error gets smaller by using more filters since it becomes easier to adapt the transmitted spectrum of two elements with nearby K-edges when the distance in energy between the edges decreases.

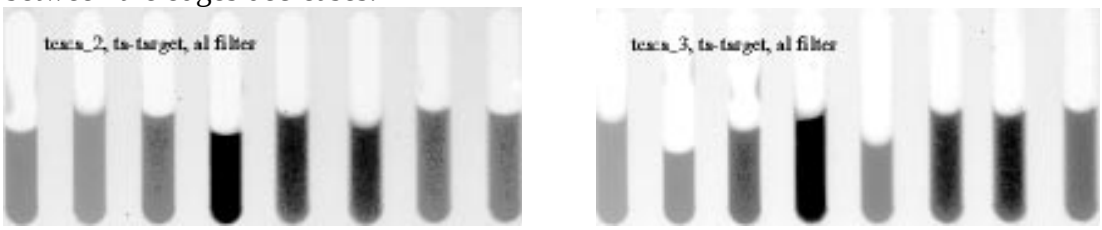

Figure 7-13. The digital image of the two TCA:s. X-rays from a tantalum target without filtering.

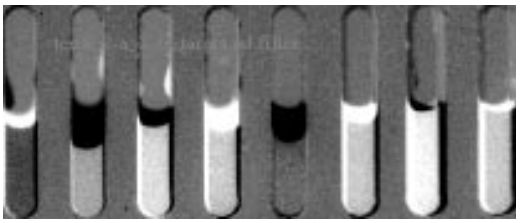

Figure 7-14. The subtracted digital image, i.e. TCA:2 - TCA:3. The lightest fields represent highest intensity. There are small areas on the sides of the cells and in the middle of the cells, which are either black or white, because of geometrical mismatch. This is also seen in some of the following subtracted pictures.

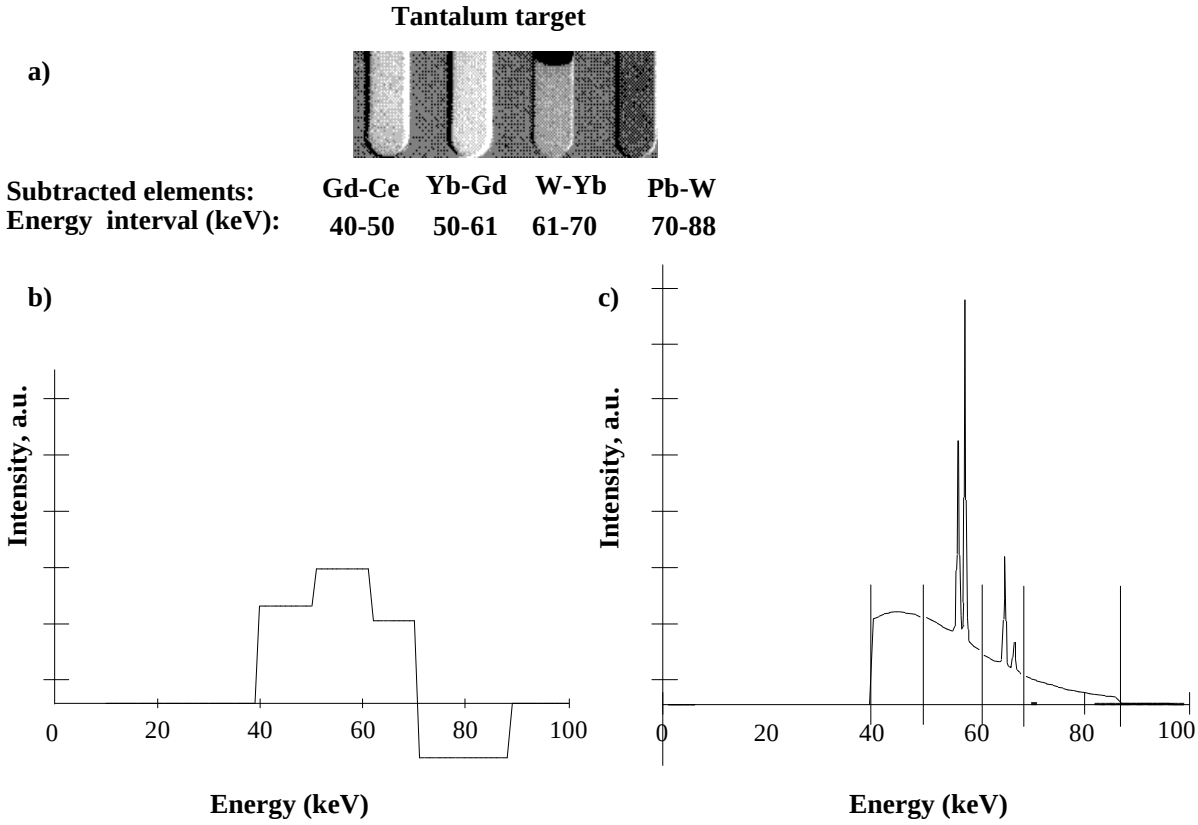

Figure 7-15. Tantalum target without filtering. a) The spectrum is divided into four intervals determined by the K-edges of the elements used in the TCA:s. The subtracted digital picture, the four intervals and the elements are shown in the figure. b) A spectrum in histogram form is reconstructed. The pixel values from each TCA are converted into PSL-values, averaged and subtracted with help of the programme. c) A modelled spectrum from a tantalum target.

Tantalum target Gadolinium filter

a)

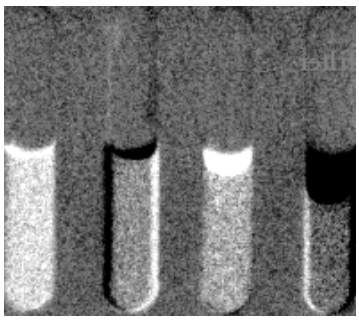

Subtracted elements:	**Gd-Ce**	**Yb-Gd**	**W-Yb**	**Pb-W**	
Energy interval (keV):	**40-50**	**50-61**	**61-70**	**70-88**	**(keV)**

b)

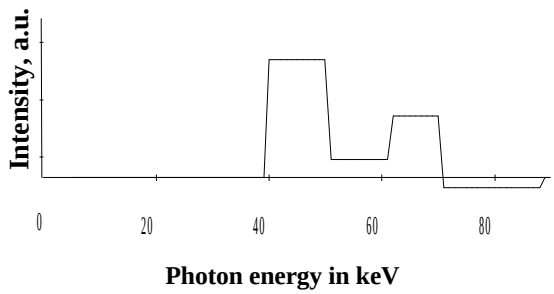

c)

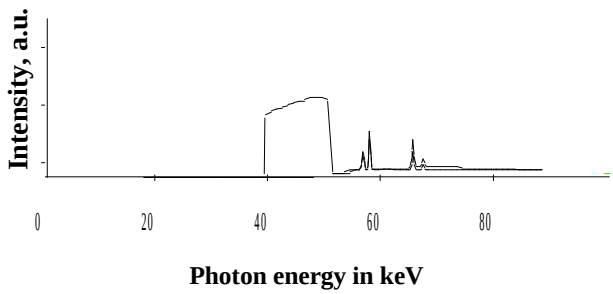

Figure 7-16. Tantalum target filtered with gadolinium. a) The subtracted digital picture, the elements and the four intervals. b) A reconstructed spectrum in histogram form. c) A modelled spectrum from a tantalum target filtered with gadolinium.

Tantalum target Tantalum filter

a)

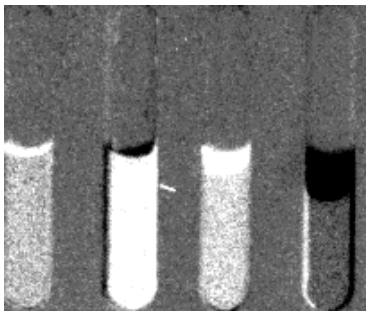

Subtracted elements:	**Gd-Ce**	**Yb-Gd**	**W-Yb**	**Pb-W**	
Energy interval (keV):	**40-50**	**50-61**	**61-70**	**70-88**	**(keV)**

b)

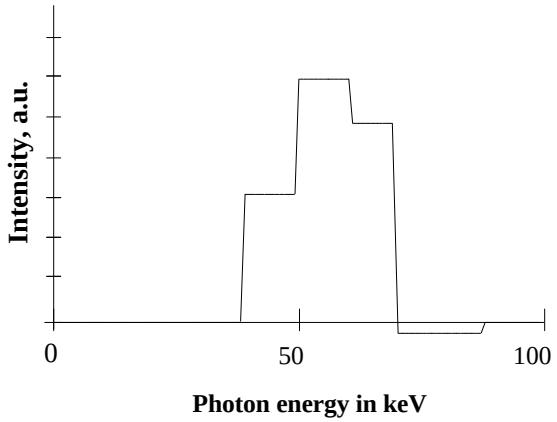

c)

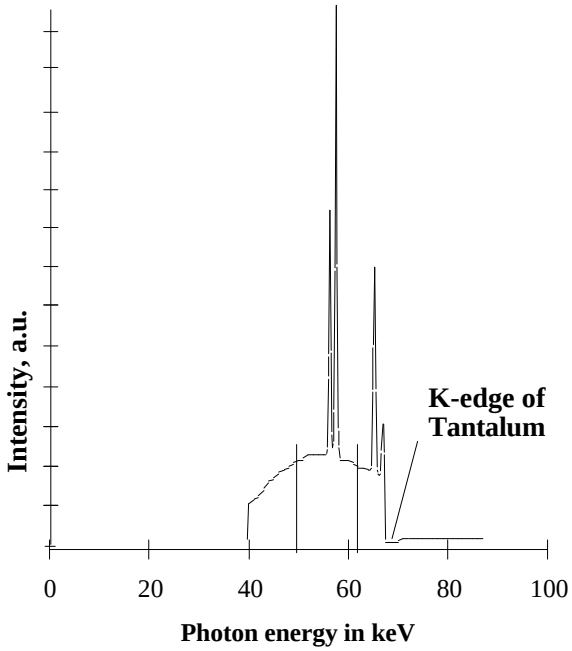

Figure 7-17. Tantalum target filtered with tantalum. a) The subtracted digital picture, the elements and the four intervals. b) A reconstructed spectrum in histogram form. c) A modelled spectrum from a tantalum target filtered with tantalum.

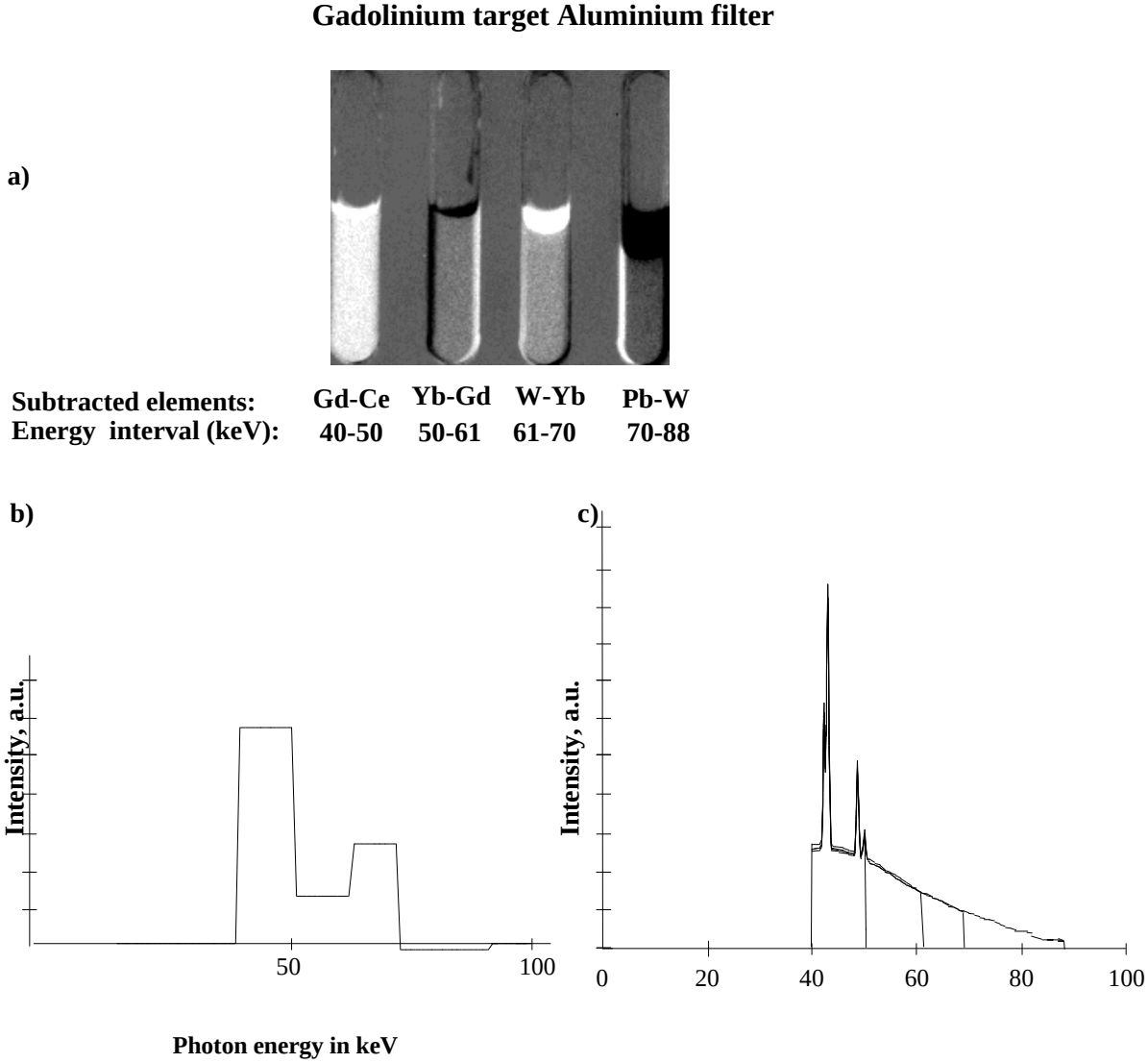

Figure 7-18. Gadolinium target filtered with aluminium. a) The subtracted digital picture, the elements and the four intervals. b) A reconstructed spectrum in histogram form. c) A modelled spectrum from a gadolinium target filtered with aluminium.

7.4 X-ray tube

X-rays are emitted when fast moving electrons are decelerated in the target anode of an evacuated X-ray tube. The spectrum consists of a Bremsstrahlung continuum and discrete characteristic lines. The target material is frequently tungsten, though other elements are also used such as molybdenum. Such a spectrum with emission lines is shown in Fig. 7-19. The energy range of the Bremsstrahlung spectrum can be varied by tuning the voltage over the X-ray tube and the intensity by varying the current.

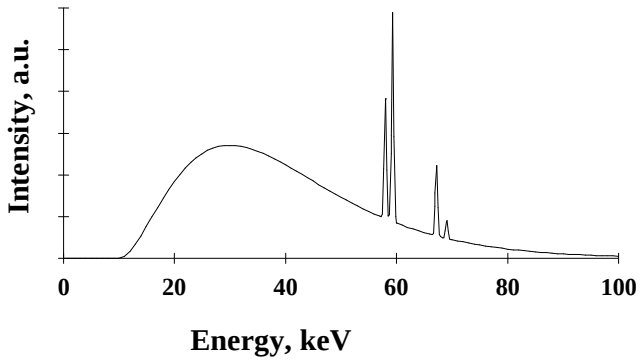

Figure 7-19. A modelled spectrum from an X-ray tube with a tungsten target.

7.4.1 Spectral measurements

The purpose of this experiment is to use our new method of spectral measurement on a known spectrum and compare the results. Two IP:s were exposed with X-rays from the X-ray tube through the filter set. Each IP was divided in four fields and exposed differently with the filter set just in front of the field. IP:1 was exposed with various voltages and IP:2 with various voltages and filtering of the X-ray radiation. The unexposed fields of the IP were protected with 50 mm thick lead bricks. The current (1mA) and exposure time (15s) was the same in all cases (see Table 7-4).

IP:1				
Field:	1	2	3	4
Voltage (kV):	110	100	80	60

IP:2				
Field:	5	6	7	8
Voltage (kV):	80	100	80	100
Filter:	Ta	Ta	Gd	Gd

Table 7-4. The different fields with exposure of the two IP:s.

The eight spectra were also measured with a conventional Ge-detector and saved in a file. The spectra measured with the differential absorption method are compared with the spectra measured with the detector in Fig. 7-20 - 7-22. The subtracted pictures are also shown in the figures. The negative area in the histogram can be the result of having solutions that are not perfectly matched, i.e. transmission errors.

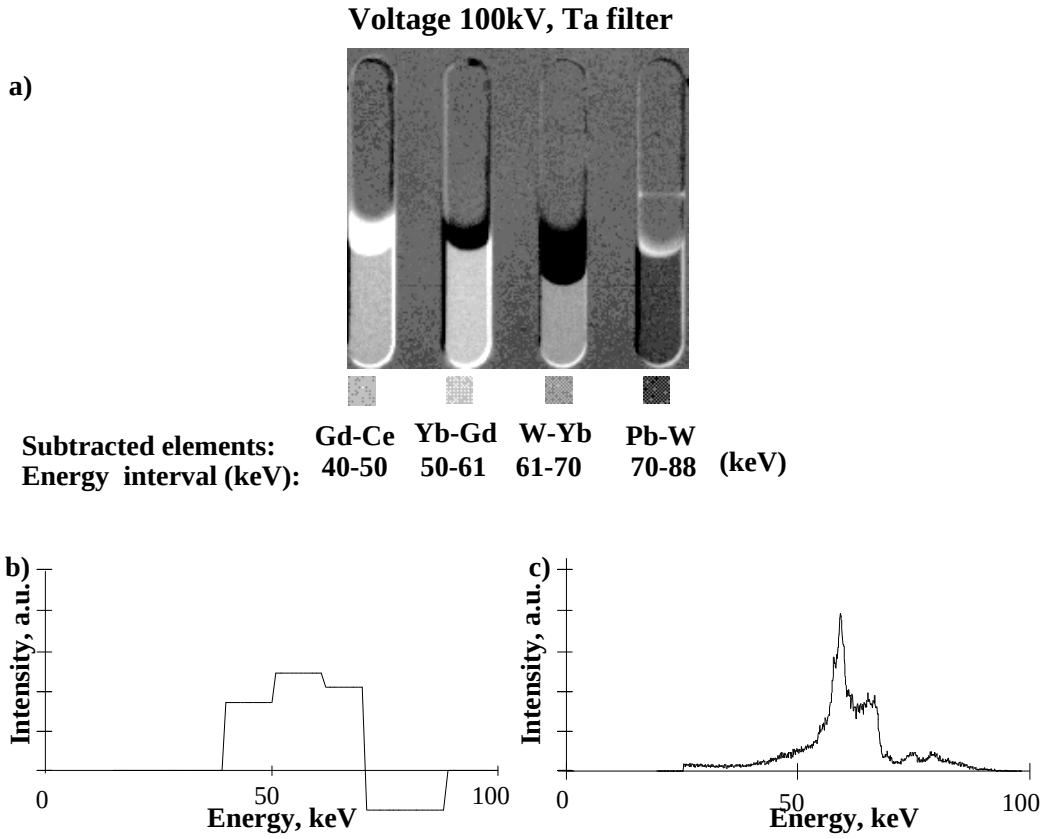

Figure 7-20. X-ray tube with a voltage of 100 kV and a current of 1mA, filtered with tantalum. a) The subtracted digital picture, the elements and the four intervals. b) A reconstructed spectrum in histogram form. c) The spectrum measured with a Ge-detector.

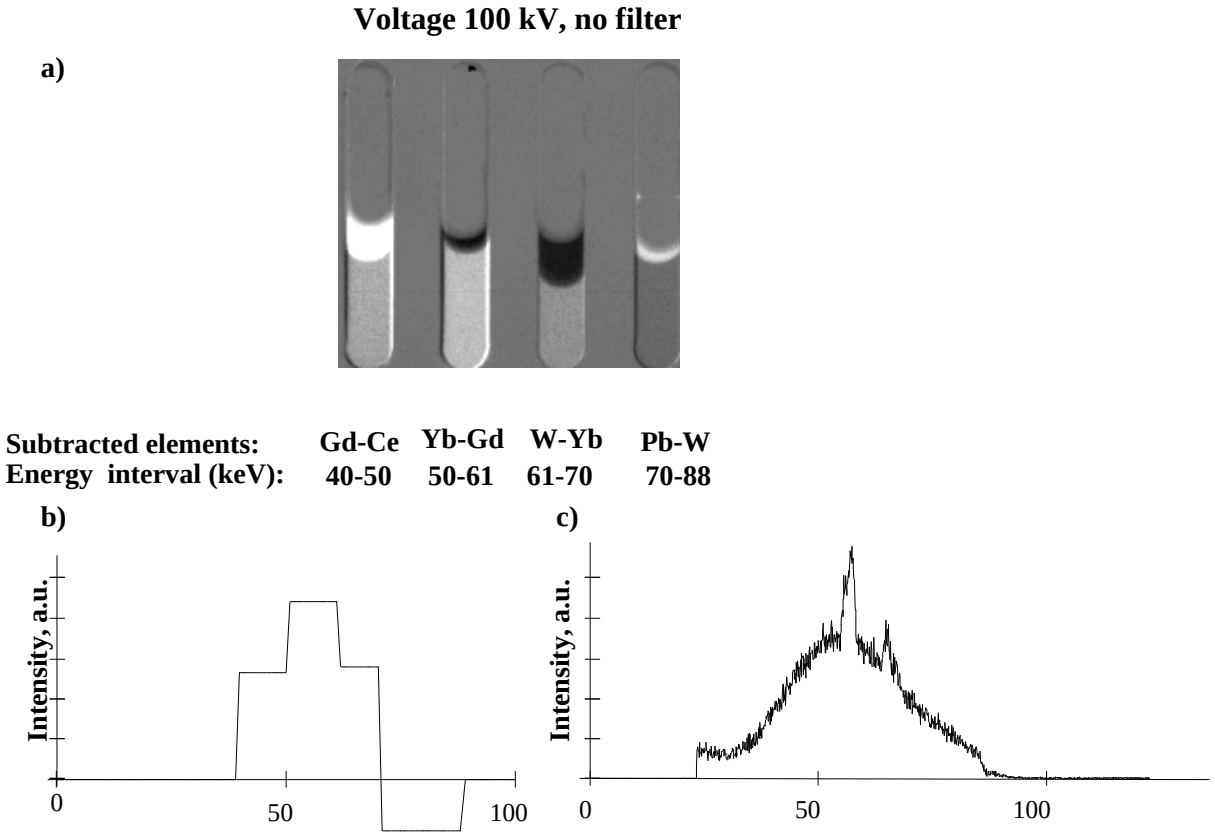

Figure 7-21. X-ray tube with a voltage of 100 kV and a current of 1mA. a) The subtracted digital picture, the elements and the four intervals. b) A reconstructed spectrum in histogram form. c) The spectrum measured with a Ge-detector.

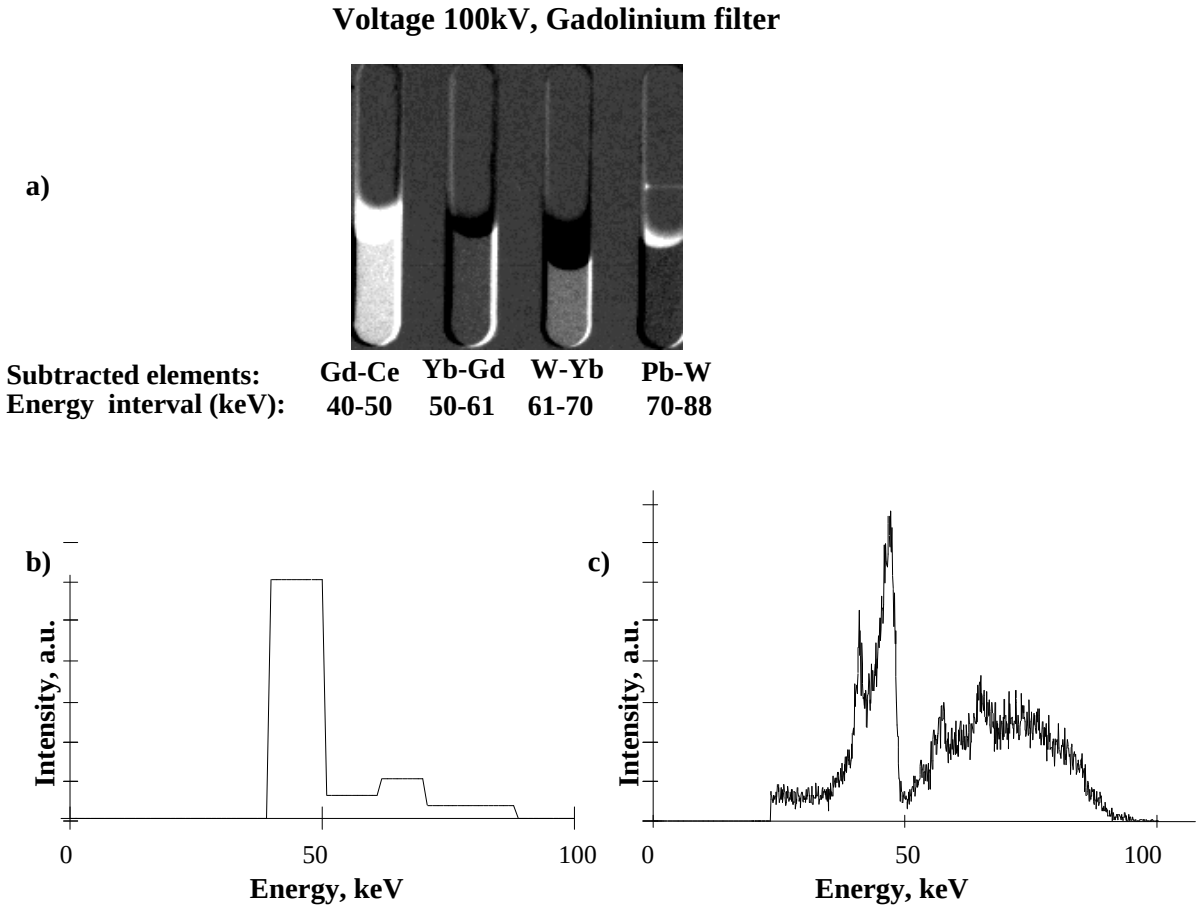

Figure 7-22. X-ray tube with a voltage of 100 kV and a current of 1mA, filtered with gadolinium. a) The subtracted digital picture, the elements and the four intervals. b) A reconstructed spectrum in histogram form. c) The spectrum measured with a Ge-detector.

8. Summary

The aim of this work has been to evaluate a new method of measuring spectra from laser-produced plasmas by differential absorption. Measurement with this new method have been done with a mono-energetic iodine source, a polychromatic X-ray source based on a laser-produced plasma with different filtering and a conventional X-ray tube. The result was satisfactory, e.g. it was possible to identify the different spectra. The accuracy was relatively low since only five different elements were used and the spectrum was divided in four intervals. The resolution was ≈ 10 keV because the distance in energy between the K-edges of nearby elements was 10 keV. The examined spectral range was 40 keV to 88 keV. The relative transmission error was around 10 -15 % which led to spectral intensity errors of 14-20 %. The largest error contribution came from the standard deviation of the grey scale values on the image plate that is proportional to the exposure of the image plate. Having a well-adapted exposure time i.e. not too high (leading to over exposure of the IP) and not too low (leading to large standard deviations of the grey scale values), this error could be decreased to <1% (Sect. 4). The error in concentration could also be less using better chemical instruments when mixing the solutions. The resolution and energy range are determined by the elements used. It is possible to examine an energy range up to 116 keV with a resolution of 2 keV by using more elements.

9. Acknowledgements

First, I would like to thank my supervisor Carl Tillman who helped me a lot through the diploma work. I would also like to thank Ian Mercer whose knowledge's I could not be without and Mattias Grätz who helped me with the programming part. Bertil Hermansson who helped me with my hardware problems and Alice, born in the middle of the work, who was a very nice baby and let me work. Finally, I would like to thank Sune Svanberg for being my examiner and all the people at the Department of Physics in Lund.

10. References

1. K. Herrlin, G. Svahn, C. Olsson, H. Pettersson, C. Tillman, A. Persson, C.-G. Wahlström and S. Svanberg, *Generation of X-rays for Medical Imaging by High-Power Lasers: Preliminary Results*, Radiology **189**, 65-68, 1993.
2. W.C. Röntgen, *Sitzungsberichten der Physikal.-Medicin.* Gesellschaft 132 (Würzburg 1895), English translation in Nature **53**, 274, 1896.
3. S. Svanberg, *Atomic and Molecular Spectroscopy*, Springer-Verlag, New York, 1992.
4. J.D. Kmetec, *Ultrafast Laser Generation of Hard X-Rays*, Thesis, Stanford University, 1992.
5. P.K. Carrol and E.T Kennedy, *Laser-Produced Plasmas*, Contemp. Phys, 1981, No. 1, 61-96.
6. H. Haken and H.C. Wolf, *Atomic and Quantum Physics*, Springer-Verlag, Berlin, 1987.
7. T. Hamaoka, *Autoradiography of new Era Replacing Traditional X-Ray Film - Bio-Imaging Analyser BAS2000*, Cell Technology, **9**, 456-462, 1990.
8. J. Miyahara, *The Imaging Plate: A New Radiation Image Sensor*, Chemistry Today, October, 29-36, 1989.
9. G. Blom, *Sannolikhetsteori med Tillämpningar*, Studentlitteratur, Lund, 1984.
10. WM.J. Veigele, *Photon Cross Section from 0.1 keV to 1 MeV for Elements Z = 1 to Z = 94*. Atomic Data, **5**, 51-111, 1973.
11. S. Svanberg, J. Larsson, A. Persson and C.-G. Wahlström, *Lund High-Power Laser Facility - System and First Results*, Physica Scripta **49**, 187-197, 1994.
12. C. Tillman, I. Mercer and S. Svanberg, *Elemental Biological Imaging by Differential Absorption Using a Laser-Produced X-ray Source*, Jour. Opt. Soc. Am. B **13**, 1996.
13. C. Tillman, A. Persson, C.-G. Wahlström, S. Svanberg and K. Herrlin, *Imaging Using hard X-rays from a Laser-produced Plasma*, Applied Physics B **61**, 333-338, 1995.
14. R.C. Weast (ed.), *Handbook of Chemistry and Physics*, 54th edition, CRC Press, Cleveland, Ohio, 1973-1974.
15. C. Andersson, *Differential Imaging using Hard X-rays from Laser-Produced Plasma*, LRAP-174, Lund Institute of Technology, 1995.

Appendix A

```
Program CCD_XRay_Spectra(infile,outfile,input,output);

Uses   WinCrt,WinProcs, WinTypes, WinDos, WinAPI, Strings, Objects;
{$DEFINE _test_output }
(* remove the first underscore to see the Header's File Informations *)
Const
  ImageMaxSize      = 2048;

Type
  X_Col          = array[1..ImageMaxSize] of byte;

Var
  Filename                                        : String;
  Image                                           : array[1..ImageMaxSize] of ^X_Col;
  BMIHead                                         : TBitmapFileHeader;
  BMPHead                                         : TBitmapInfoHeader;
  AnyPointer                                      : Pointer;
  Hand                                            : THandle;
  maxpix,minpix,i,
  xmax,ymax,xmin,ymin,k,psl,rad,kol,l,s      :integer;
  ch                                               : char;
  medelvarden, medelvarden2                        :array[1..100] of real;
  psl0                                             :real;
  datafile                                        :text;

Procedure ReadImageFile(Dir : String);

(*Reads all information in the raw image*)

var
  col,add,loop              : Integer;
  Read_Bytes,y                : Word;
  FileHandle                : THandle;
  PFName                    : PChar;
  {$IFDEF test_output}
    ch                      : Char;
    Y_Pos                   : Byte;
  {$ENDIF}

 Begin
  {$IFDEF test_output}
    Writeln('Momentarily read file: ',Dir);
  {$ENDIF}
  PFName:=GlobalAllocPtr(gmem_Moveable+gmem_ZeroInit,80);
  StrPCopy(PFName,Dir);
  FileHandle:=_lopen(PFName,0);
  AnyPointer:=@BMIHead;
  Read_Bytes:=_lread(FileHandle, AnyPointer, 14);
  if Read_Bytes<>14 then writeln('Some mistake in reading BMIHead');
  AnyPointer:=@BMPHead;
  Read_Bytes:=_lread(FileHandle, AnyPointer, 40);
  if Read_Bytes<>40 then writeln('Some mistake in reading BMPHead');
  {$IFDEF test_output}
    WriteLn;
    Writeln('Output of the BMI-Header:');
    With bmihead do
      begin
        Writeln('BMFTYPE:     ',chr(bfType mod 256),chr(bfType div 256));
        Writeln('BMSize:      ',bfSize);
                WriteLn('BFRESERVED1: ',bfReserved1);
                WriteLn('BFRESERVED2: ',bfReserved2);
                WriteLn('BFOffBits:   ',bfOffBits);
      end;
    With bmphead do
      begin
        WriteLn('BiSize:      ',BISIZE);
                WriteLn('BiWidth:     ',BiWidth);
                WriteLn('BiHeight:    ',BiHeight);
                WriteLn('BiPlanes:    ',BiPlanes);
                WriteLn('BiBitCount:  ',BiBitCount);
                WriteLn('BiSizeImage: ',BiSizeImage);
                WriteLn('BiXPelsPerm: ',BiXpelsPerMeter);
                WriteLn('BiYPelsPerm: ',BiYpelsPerMeter);
```

```
                WriteLn('BiClrUsed:   ',BiClrUsed);
     end;
   repeat ch:=readKey; until ch<>'';
  {$ENDIF }
  AnyPointer:=GlobalAllocPtr(gmem_Moveable+gmem_ZeroInit,2048);
  Read_Bytes:=_lread(FileHandle,AnyPointer,BMIHead.bfOffBits-54);
     (* Just Skip the Color-Information, using bfOffBits *)
  Hand:=GlobalFreePtr(AnyPointer);
  if Read_Bytes<>(BMIHead.bfOffBits-54)
   then writeln('Some mistake in reading the whole RGB Information');
  WriteLn('Reading Data....');
  Writeln('Width: ',BMPHead.Biwidth);
  WriteLn('Height: ',BMPHead.Biheight);
  col:=BMPHead.BiWidth;
  add:=col mod 4; if add=0 then add:=4;          (* This procedure is important, because    *)
  col:=col+(4-add);                              (* Width must be a multiple of 4 for BMP's *)
  Writeln('Width to be read: ',col);
  {$IFDEF test_output}
   Y_Pos:=WhereY;
  {$ENDIF}
  for y:= 1 to BMPHead.BIHEIGHT do
   begin
    {$IFDEF test_output}
     Y_Pos:=WhereY;
                GotoXY(0,Y_Pos);
                Write('Row: ',y);
      if y=BMPHead.BIHEIGHT then WriteLn;
    {$ENDIF}
    Image[y]:=GlobalAllocPtr(gmem_Moveable+gmem_ZeroInit,col);
    anypointer:=Image[y];
    Read_Bytes:=_lread(FileHandle,Anypointer,col);
    if Read_Bytes<>(col) then
          writeln('Something went wrong in reading this BMP-Line (',Read_Bytes,' Bytes Read)');
   end;
  Read_Bytes:=_lclose(FileHandle);
end; (*ReadRawImage*)

procedure readkoord(var xmin,ymin,xmax,ymax:integer);
  var goon:boolean;
  begin
    goon:=false;
    while not goon do
    begin
     writeln('ange koord x1');
     readln(xmin);
     writeln('ange koord y1');
     readln(ymax);
     writeln('ange koord x2');
     readln(xmax);
     writeln('ange koord y2');
     readln(ymin);
     if (xmin>xmax) or (ymax>bmphead.biheight) or (xmax>bmphead.biwidth) or (ymin>ymax) then
       goon:=false
     else
       goon:=true;
    end;
   end;(*readkoord*)

function medelvarde(xmin,ymin,xmax,ymax,l:integer; psl0:real):real;
(*gives the meanvalue of the psl-values in a given area minus the 'zeropsl'*)
  var summa,psl,pslbg,sum:real;
      ant,rad,kol:integer;
  begin
  summa:=0;
  sum:=0;
  ant:=0;
 (*writeln(BMPHead.biheight-ymax);
  writeln(BMPHead.biheight-ymin); *)
  for rad:=BMPHead.biheight -ymax +1  to BMPHead.biheight - ymin do
  begin
    for kol:= xmin + 1 to xmax do
    begin
      psl:=Image[rad]^[kol];
      sum:=sum+psl;
      (*write(round(psl));
      write(' ');*)
```

```
      psl:=((psl*(maxpix-minpix)/255+minpix)/1024)- 0.5;
      psl:=10000/s*exp(l*psl*ln(10));
      psl:=psl-psl0;
      summa:=summa+psl;
      inc(ant);
    end;
   (* writeln; *)
  end;
  writeln(ant);
  summa:=summa/(ant);
  write('mean-psl=');
  writeln(summa);
  sum:=sum/ant;
  write('meanpixvalue=');
  writeln(sum);
  medelvarde:=summa;
  end;(*medelvarde*)

begin (*Main program*)
(* StrCopy(WindowTitle,'CCD - X-Ray - Evaluation');*)
 (* InitWinCrt;*)
  WriteLn('Which files would you like to chose in this directory (including wildcards)');
  ReadLn(FileName);
  ReadImageFile(FileName);
  writeln('write maxpixelvalue');
  readln(maxpix);
  writeln('write minpixelvalue');
  readln(minpix);
  writeln('write latitud');
  readln(l);
  writeln('write sensitivity');
  readln(s);
  writeln('do you want to subtract the zerolevel-pslvalues from your picture?y/n');
  readln(ch);
  if ch='y' then
  begin
     write('write koord from unexposed IP(under leadbrick)');
     readkoord(xmin,ymin,xmax,ymax);
     psl0:=medelvarde(xmin,ymin,xmax,ymax,l,0);
  end
  else
     psl0:=0;
  ch:='y' ;
  k:=0;
 (* for rad:=1 to BMPHead.biheight do
  begin
    for kol:= 1 to BMPHead.biwidth do
    begin
       psl:=Image[rad]^[kol];
       write(round(psl):4);
    end;
    writeln;
  end; *)
  while ch <>'n' do
  begin
    inc(k);
    readkoord(xmin,ymin,xmax,ymax);
    medelvarden[k]:=medelvarde(xmin,ymin,xmax,ymax,l,0);
    medelvarden2[k]:=medelvarde(xmin,ymin,xmax,ymax,l,psl0);
    writeln('do you want to continue? y/n');
    readln(ch);
  end;
  writeln('write outfilename');
  readln(filename);
  assign(datafile,filename);
  rewrite(datafile);
  for i:=1 to k do
  begin
     write(datafile, medelvarden[i]);
     write('    ');
     writeln(datafile, medelvarden2[i]);
  end;
  close(datafile);
  Writeln('End.');
end.
```